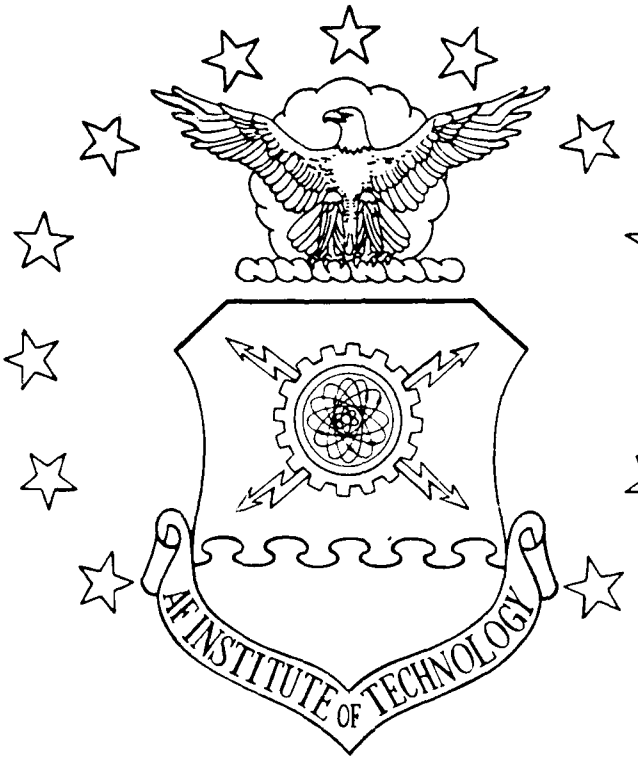

EFFECT OF RIBLETS ON FLOW SEPARATION FROM A CYLINDER AND AN AIRFOIL IN SUBSONIC FLOW

THESIS

Timothy D. Wieck
Captain, USAF

AFIT/GAE/ENY/89D-40

DEPARTMENT OF THE AIR FORCE
AIR UNIVERSITY
AIR FORCE INSTITUTE OF TECHNOLOGY

Wright-Patterson Air Force Base, Ohio

AFIT/GAE/ENY/89D-40

EFFECT OF RIBLETS ON FLOW SEPARATION FROM A CYLINDER AND AN AIRFOIL IN SUBSONIC FLOW

THESIS

Presented to the Faculty of the School of Engineering

of the Air Force Institute of Technology

Air University

In Partial Fulfillment of the

Requirements for the Degree of

Master of Science in Aeronautical Engineering

Timothy D. Wieck, B.S.

Captain, USAF

December 1989

Preface

The purpose of this thesis was to investigate the effects of riblets on delaying flow separation from a cylinder and an airfoil in subsonic flow. Riblets have been used successfully in the past to reduce viscous drag and delay separation in a two-dimensional, straight-walled, subsonic diffuser.

This thesis, as with most projects or programs, was not the work of one individual and I would like to recognize those who gave support, both technical and moral, throughout this project. First and foremost, I would like to thank my thesis advisor, Lt Col Paul I. King, whose knowledge and guidance were essential to the success of this project. I would also like to thank my thesis committee, Dr. W. C. Elrod and Dr. M. E. Franke, for their technical advise and inputs. Thank you also to lab supervisor, Mr. Nicholas Yardich, and technicians Andy Pitts, Mark Derriso, Dan Rioux, and Jay Anderson for everything from hunting down various supplies to replacing a wind tunnel shaft bearing. Thanks also to Jack Tiffany and Dave Driscol of the Fabrication Division for building the boundary layer probe, refurbishing the models, and servicing the traversing device.

On the home front, special thanks to wife, Marla, and daughter, Mariah, for providing moral support and encouragement throughout this endeavor.

Timothy D. Wieck

Table of Contents

List of Figures

List of Tables

List of Symbols

Symbol		Units
AOA	angle of attack	deg
c	chord length	ft
C_f	local skin friction coefficient	none
C_p	pressure coefficient	none
h	riblet peak-to-valley height	ft
h^+	nondimensional riblet height	none
H	turbulent boundary layer shape factor	none
H	diffuser throat height	none
L	surface distance from leading edge to trailing edge	none
o.d.	outside diameter	ft
P	pressure	lb_f/ft^2
P_t	total pressure	lb_f/ft^2
P_s	static pressure	lb_f/ft^2
q	dynamic pressure	lb_f/ft^2
Re	Reynold's number	none
Re_x	local Reynold's number	none
s	riblet peak-to-peak width	ft
s^+	nondimensional riblet width	none
t	airfoil model thickness	ft
U	local flow velocity	ft/sec
U_ϵ	boundary layer edge velocity	ft/sec
U_τ	friction velocity	ft/sec

U_∞	freestream velocity	ft/sec
V	velocity	ft/sec
$w(y/\delta)$	Cole's wake function	none
X	distance from leading edge along surface	ft
X_{sep}	separation location measured from leading edge along surface	ft
x	distance from leading edge along chord line ...	ft
y	local height	ft
y^+	nondimensional local height	none
α	angle of attack	deg
δ	local boundary layer thickness	ft
δ^*	displacement thickness	ft
δ_l	local viscous sublayer thickness	ft
ϵ	error parameter	none
ϵ_{rms}	root-mean-square-error	none
η	nondimensional laminar boundary layer coordinate	none
θ	momentum thickness	ft
θ	diffuser divergence half-angle	deg
κ	von Karman's mixing length constant	none
μ	viscosity	lb_f•sec/ft
ν	kinematic viscosity	ft^2/sec
$\Pi(x)$	Cole's profile parameter	none
ρ	density	$slug/ft^3$
τ_w	wall shear	lbf/ft^2
$\phi_1(y^+)$	turbulent boundary layer law-of-the-wall function	*none*
ϕ	angle between leading edge and point on cylinder with vertex at center of cylinder	deg

ϕ_{sep}	angle between leading edge and separation point with vertex at center of cylinder	deg
$\Delta\phi_{sep}$	change in separation angle	deg

Abstract

The purpose of this thesis was to investigate the effect of riblets on flow separation from a cylinder and an airfoil in subsonic flow. Riblets have been used successfully to reduce viscous drag on a flat plate and significantly delay flow separation in a two-dimensional, straight-walled, subsonic diffuser.

The investigation indicated that for a 2-D cylinder model, the separation point could be delayed as much as 5.5 percent by applying riblets to the model surface. Minor delays in separation were also achieved by applying riblets to a 2-D airfoil model at 8 and 12 deg angle of attack.

Applying riblets to the cylinder and airfoil models consistently altered the pressure distribution compared to the same models without riblets. In comparing the cylinder and airfoil results with those of the subsonic diffuser, it appears that riblets are most effective in delaying flow separation in relatively weak adverse pressure gradients.

I. Introduction

The purpose of this thesis was to experimentally investigate the effect of riblets upon flow separation from a cylinder and an airfoil having turbulent boundary layers in subsonic flow. Riblets are small flow-aligned grooves which can be attached to an aerodynamic surface. Previous studies have centered primarily on viscous drag reduction, but a recent report investigated the effect of riblets on flow separation in a two-dimensional, straight-walled, subsonic diffuser (Martens, 1988:58-59). The location of flow separation varied with diffuser geometry and velocity, but the use of riblets generally delayed separation, in some cases by as much as 250 percent. Since delaying separation is as important on external aerodynamic surfaces as it is in a diffuser, the objective of this thesis was to investigate whether similar marked delays in flow separation could be achieved on two aerodynamic bodies, namely the two-dimensional cylinder and airfoil.

II. Theory

Boundary Layers

Recall from two-dimensional potential flow theory, which makes the assumption that the fluid is inviscid, that there is no lift or drag for a cylinder in uniform flow. In addition, and of primary concern to this experiment, there is no separation at any point other than the stagnation point at the trailing edge of the cylinder. Likewise for the airfoil, there is no separation point at any location other than the trailing edge since the Kutta condition, which states that the velocity must be zero at the trailing edge, must be satisfied (Karamcheti, 1980:469). This entire experiment then hinges on the fact that real world fluids have viscosity and it is the viscous flow effects which lead to this phenomenon called separation.

For fluids of small viscosity, the effects of viscosity on the flow around streamlined bodies are concentrated in a thin boundary layer (Kuethe and Chow, 1976:299). Within the boundary layer, the flow can be laminar, turbulent, or in a state of transition between laminar and turbulent. Laminar flow occurs at low Reynolds number and is characterized as a relatively thin layer with limited momentum transfer and free from any eddying motion. This results in a relatively low velocity gradient near the wall and correspondingly low skin friction. The turbulent boundary layer is characterized by the presence of a large number of relatively small eddies. These eddies produce a transfer of momentum from the relatively fast moving outer

region of the boundary layer to the region closer to the surface. Consequently, the turbulent boundary layer is thicker and the average velocity near the surface is higher than for a laminar boundary layer, resulting in higher values of skin friction (Abbott and von Doenhoff, 1959:105).

The mixing or eddying motion of the turbulent boundary layer causes fluctuations in the flow velocity within the turbulent boundary layer. These fluctuations restrict the investigation to the values of the mean velocity across a turbulent boundary layer. Figure 1 gives the mean velocity distribution across a turbulent boundary layer for flow over a flat plate. A general conclusion that may be drawn from this figure is that it is impossible to describe the flow phenomena in the entire boundary layer in terms of one single set of parameters, as is done in the laminar flow case. As a result, it is necessary to treat a turbulent boundary layer as a composite layer consisting of inner and outer regions (Cebeci and Smith, 1974:94). The inner region is only 10-20 percent of the entire boundary layer thickness and is further divided into the viscous (or laminar) sublayer, the transitional region (buffer layer), and the fully turbulent region (see Figure 1). For the inner region it is generally assumed that the mean velocity distribution is completely determined by the wall shear, τ_w, density, ρ,viscosity, μ, and the distance from the wall. It is given by the following known as the "law of the wall" (Cebeci and Smith, 1974:95):

$$U^+ = U/U_\tau = \phi_1(y^+) \qquad (1)$$

where

$$U_\tau = \text{friction velocity} = (\tau_w/\rho)^{1/2} \quad (2)$$

$$\phi_1 = \text{mean velocity distribution} \quad (3)$$

$$y+ = yU_\tau/\nu \quad (4)$$

An important parameter that will become very important in the discussion of riblet sizing is the thickness of the laminar or viscous sublayer, δ_1, which from experiments is found to be approximately $\delta_1 = 4\nu/U_\tau$ (Kuethe and Chow, 1976:389).

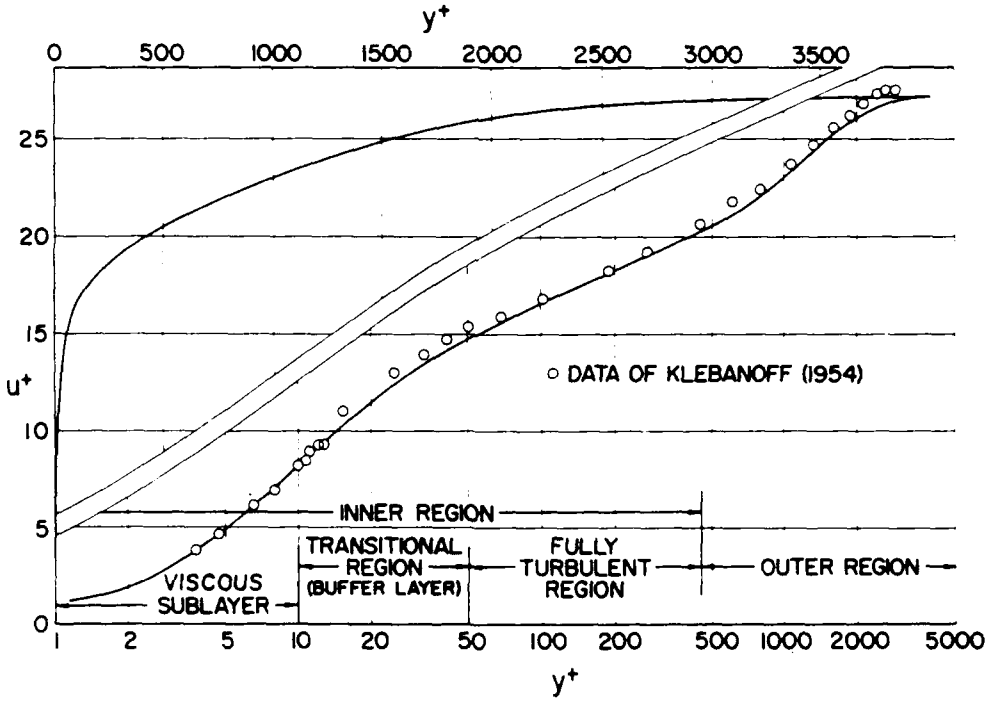

Fig. 1. Semilog and Linear Plots of Mean Velocity Distribution across a Turbulent Boundary Layer with Zero Pressure Gradient (Cebeci and Smith, 1974:94)

Flow Separation

The primary emphasis of this investigation is on delaying flow separation. Consequently it may be helpful to examine just what is meant by flow separation and to identify any problems that may be encountered when trying to determine this phenomenon experimentally.

Separation takes place only in an adverse pressure gradient ($\delta P/\delta X > 0$) and then only if the adverse pressure gradient persists over a great enough length, the length being greater the more gentle the gradient (Kuethe and Chow, 1976:315). The rising pressure and corresponding retardation of the flow results in a loss of momentum of the fluid, which is especially noticeable in the vicinity of the surface where the velocity is already low. Figure 2 shows the velocity distribution in a laminar boundary layer at and in the vicinity of the separation point. At some point beyond the minimum pressure point, point A in Figure 2, the point is reached where $\delta U/\delta y = 0$ at the wall and beyond this point the direction of the flow reverses near the surface. The point at which $\delta U/\delta y = 0$ is defined as the separation point, point B in Figure 2. The greater the magnitude of the adverse pressure gradient, the shorter will be the distance between the minimum pressure point and the separation.

The separation point in a turbulent boundary layer, as in the laminar case, takes place only in an adverse pressure gradient. The higher velocities near the surface of the turbulent boundary layer, however, enable it to drive farther against an adverse pressure gradient than can the laminar layer (Kuethe and Chow, 1976:316).

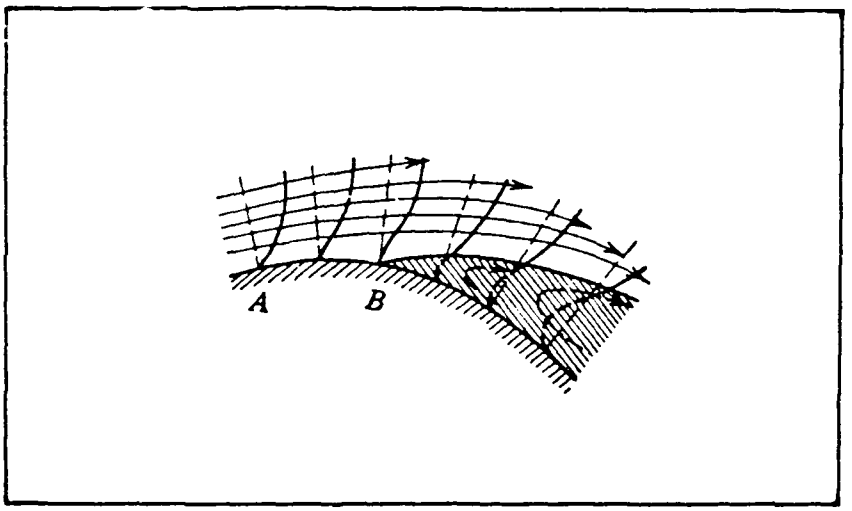

Fig. 2. Velocity Distribution in the Vicinity of the Separation Point (Kuethe and Chow, 1976:315)

To investigate turbulent separation, it is necessary to introduce the shape parameter H (Abbott and von Doenhoff, 1959:80-81,103-104):

$$H = \delta^*/\theta \tag{6}$$

where

δ^* = displacement thickness
θ = momentum thickness

Figure 3 shows the velocity distributions for various values of the shape parameter. Although it is not possible to give an exact value of H that corresponds to the turbulent separation point, separation has not been observed for values of H less than 1.8 and appears to have definitely been observed for an H of 2.6 (Abbott and von Doenhoff, 1959:103). Using an H value of 2.6 gives a baseline with which to compare experimentally collected velocity distributions and

ultimately gives a comparison curve to check the values of X_{sep} determined with oil drops or tufts.

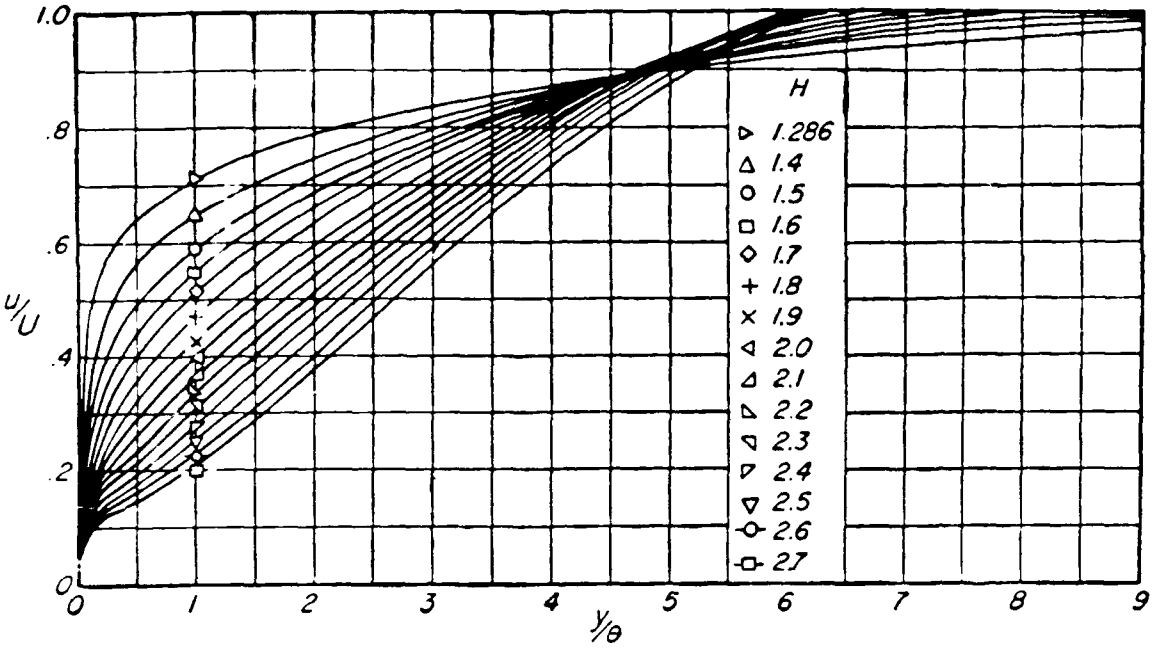

Fig. 3. Velocity Distribution in Turblulent Boundary Layers (Abbott and von Doenhoeff, 1959:104)

A complication to separation determination can occur if the separated and subsequently detached flow reattaches itself to the surface. Not much is known about the factors controlling this phenomenon, but it is most likely to occur in the case of a laminar boundary layer where downstream of the laminar separation point, the flow reattaches as a turbulent boundary layer.

Riblets

Riblets are small flow-aligned grooves that have been investigated primarily as a viscous drag reduction technique for

turbulent boundary layers. Reductions in viscous drag of up to 8 percent have been achieved with the proper geometry and scaling and the riblets were found to be insensitive to yaw angles as high as 15 deg. The scaling is done using law of the wall variables as follows (Walsh, 1982:2):

$$h^+ = (hU_e/\nu)(C_f/2)^{1/2} \quad (7)$$

$$s^+ = (sU_e/\nu)(C_f/2)^{1/2} \quad (8)$$

where

h^+ = nondimensional riblet height
h = actual riblet height
s^+ = nondimensional riblet peak-to-peak distance
s = actual riblet peak-to-peak distance
C_f = local skin friction coefficient
U_e = boundary layer edge velocity

Maximum drag reductions occurred for h^+ values between 8 and 12 and s^+ values between 15 and 20. Of all the geometries tested, two riblet configurations provided drag reductions as large as 8 percent. One was a symmetric V-groove riblet with $h^+ = s^+ = 12$ and the other was a sharp peak, significant valley curvature riblet where $h^+ = 8$ and $s^+ = 16$. While these were the optimum configurations, drag reduction still occurred whenever $h^+ < 30$ and $s^+ < 25$ (Walsh, 1982:4). The significance of the values determined for h^+ is that the actual riblet height, h, extends just above the laminar sublayer into the transitional region or buffer layer. It appears that for h^+ values beyond 30 the added wetted area counteracts any benefits realized for lower values of h^+. In the study involving the use of riblets to delay flow separation in a two-dimensional, straight-wall, subsonic diffuser, the

maximum delay in flow separation occurred with an h^+ value of 22 (Martens, 1988:59).

In the turbulent boundary layer the eddies, which cause the transfer of momentum to the region near the surface, are blamed for the greater thickness, higher mean velocity, and increased viscous drag associated with the turbulent boundary layer. One conceptual model of the structure responsible for this momentum transport is given by Wallace and Balint and is shown in Figure 4.

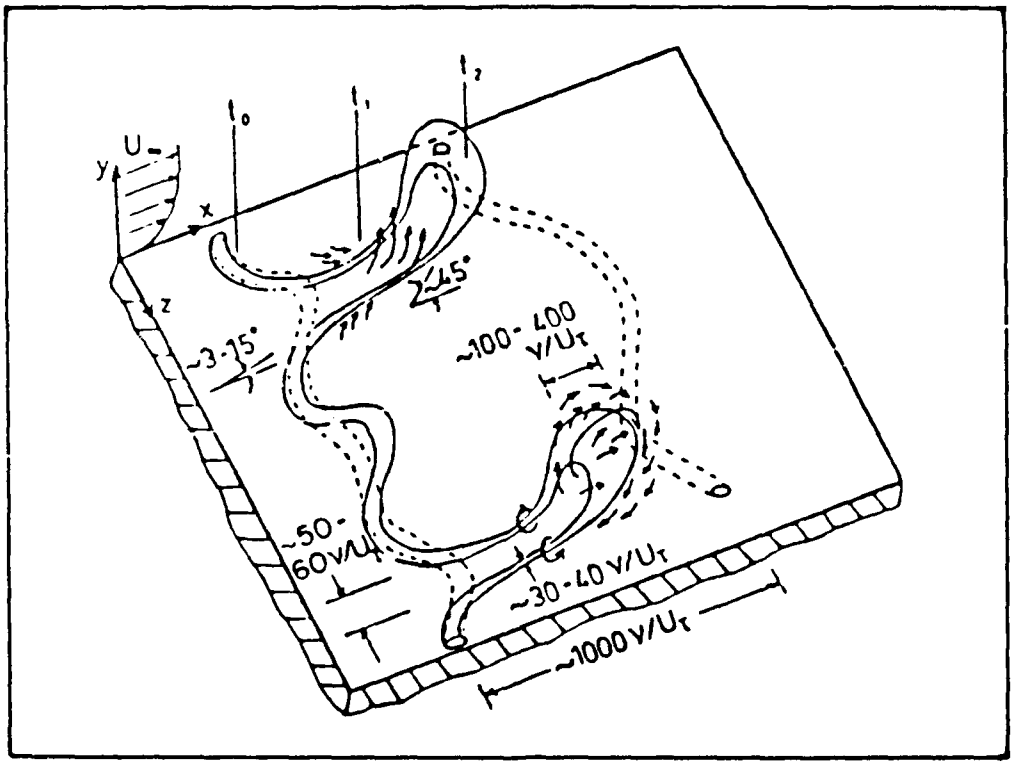

Fig. 4. Conceptual Model of Hairpin Vortices from Warped Sheets of Diffusing Vorticity
(Wallace and Balint, 1988:133)

The structure is described as a 'hairpin'-like vortex which is formed by the warped sheets of vorticity which diffuse from the

surface and are stretched downstream by the mean shear. Such structures can easily account for the 'bursting' of low momentum fluid away from the surface and 'inflow' of high momentum fluid back towards the surface, processes which are effective transporters of momentum and heat and increase surface drag (Wallace and Balint, 1988:133). It is further proposed that riblets modify and effectively reduce the momentum exchange properties caused by the streamwise vortices developing near the surface beneath a turbulent layer, with a consequent reduction in the surface shear stress (Bacher and Smith, 1986:1384). The sharp-peaked riblets are believed to limit spanwise concentration of low-speed fluid and that this is accomplished by a mechanism that depends on secondary vortex generation as shown in Figure 5. The secondary vortices should weaken the streamwise

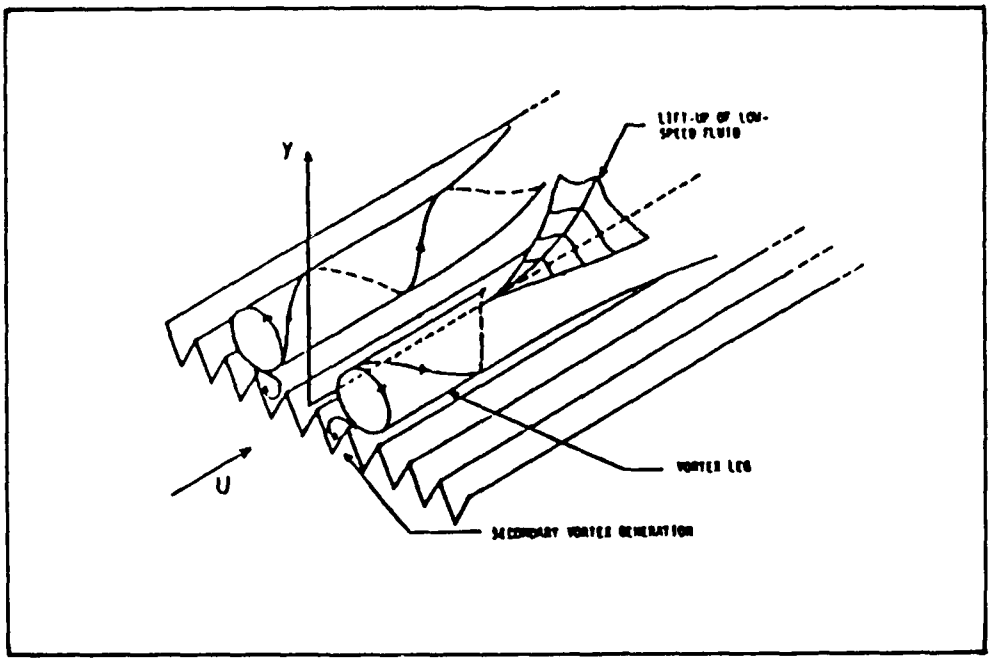

Fig. 5. Secondary Flow Generation on a Riblet Surface (Bacher and Smith, 1986:1384)

vortices and inhibit the spanwise concentration of low-speed fluid in streak formations. This should decrease the number of 'burst' sites, which will inhibit turbulent momentum exchange in the boundary layer. This process enables the riblet surface to retard the development of the turbulent boundary layer and thus to reduce the surface drag (Bacher and Smith, 1986:1384).

The theories presented to this point serve well to explain the reduction in viscous drag, but do not begin to explain why the use of riblets in a two-dimensional, subsonic diffuser can delay separation by as much as 250 percent of the diffuser wall length. The theories propose that riblets inhibit the momentum exchange in the boundary layer, yet it was this momentum exchange that increased the mean velocity near the wall and allowed the turbulent boundary layer to drive farther against an adverse pressure gradient before separating. The only explanation, and this is merely postulation, is that although the momentum transport near the surface is reduced enough to reduce the velocity gradient near the wall, the momentum must be sufficient outside the inner region to delay the separation induced by the adverse pressure gradient.

III. Experimental Apparatus

Wind Tunnel

The experimental research for this thesis was conducted in the AFIT 14-inch (35.6 cm) Wind Tunnel Facility located in Building 95A, Area B, Wright-Patterson AFB. The 680 sq ft (63 sq m) facility contains a closed-circuit wind tunnel, a Meriam Instrument Company micromanometer, an Ann Arbor Instrument Works 40-tube manometer bank, and a Precision Thermometer & Instrument Company barometer. The facility also contains a pyramidal three component force balance with an angle of attack (AOA) adjustment and a y-shaped yoke for mounting the models. Only the AOA adjustment and the model mount were used for these experiments.

An additional piece of equipment, essential to boundary layer measurements, was the probe support mechanism shown schematically in Figure 6. This device allowed both vertical and upstream/downstream traversing of the 13.75 in. (34.93 cm) diameter test section in increments of 0.001 in. (0.0254 mm). Also shown in Figure 6 are the total pressure tube and the static pressure tap locations (static taps at 1 and 2). Throughout this report P_1 and P_2 will refer to the static pressures in the low speed settling chamber and the test section, respectively.

Tunnel Models

Two different wood models were used during this experiment. The first is a pressure-tapped cylinder model measuring 2.50 in. (6.35 cm)

in diameter by 10 in. (25.4 cm) in length. The seven pressure taps on the upper half of the cylinder are spaced 30 deg. apart, beginning at the leading edge.

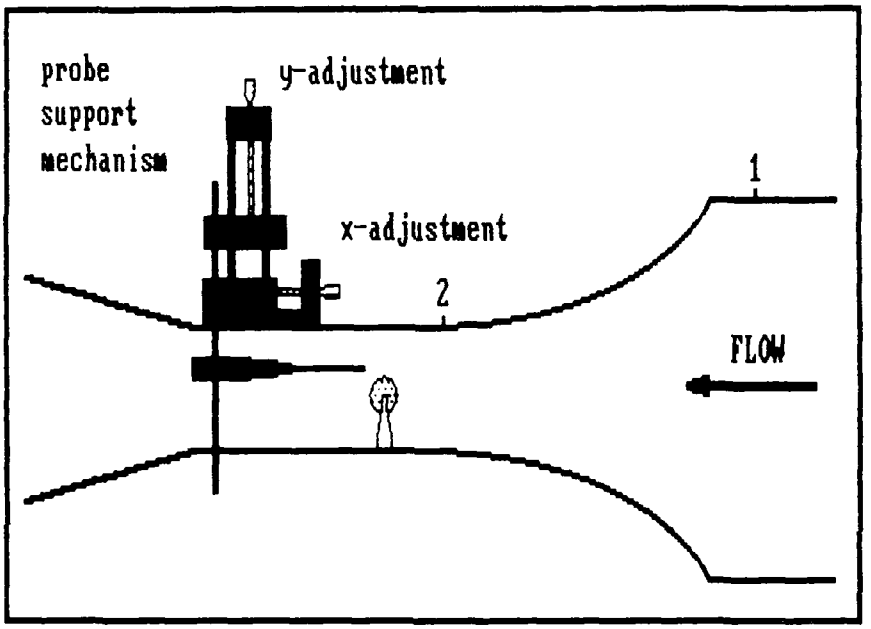

Fig. 6. Wind Tunnel Apparatus and Static Pressure Tap Locations

The second model is a NACA 64_4-021 symmetric airfoil with a chord length of 2.45 in. (6.22 cm) and a profile as shown in Figure 7. This model is also 10 in. (25.4 cm) long and is pressure-tapped with eight taps on the upper surface and seven on the lower surface. Partial blockage of a few taps was encountered leaving seven clear taps on the upper surface and five on the lower surface. (See Figure 7 for tap locations). Both the cylinder and the airfoil are 2-D models and as such are fitted with 6.0 in. (15.24 cm) diameter circular end plates.

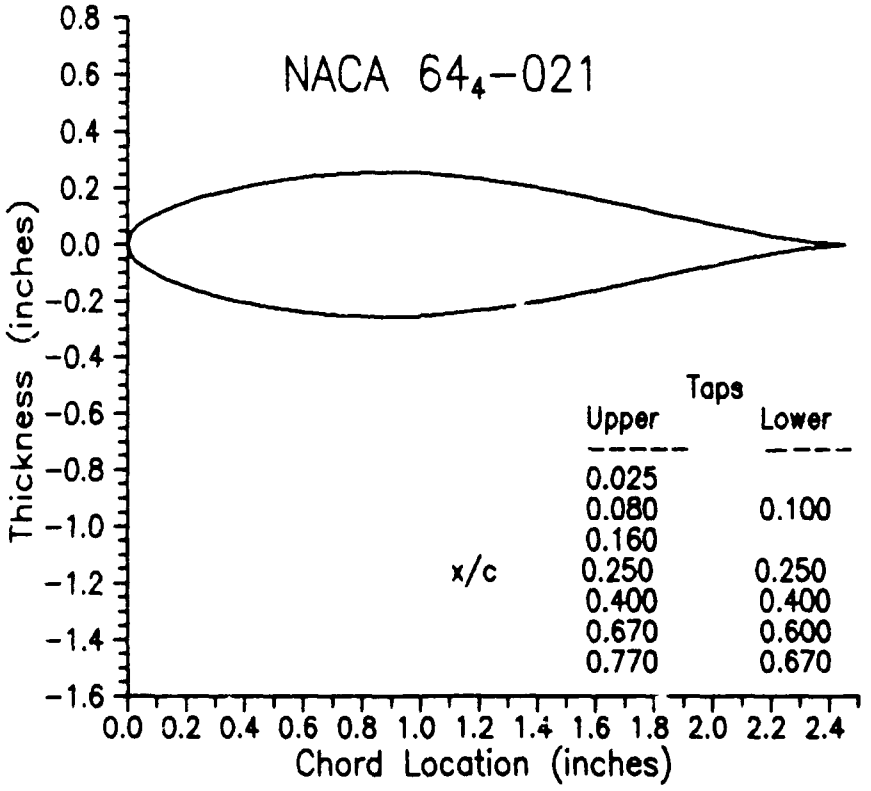

Fig. 7. NACA 64_4-021 Airfoil Profile and Model Tap Locations

A 0.4 in. (1.02 cm) wide strip of 20 squares/inch strip chart paper was fastened with adhesive tape to the surface of both models. The strip, which was wrapped around both upper and lower surfaces from leading to trailing edge, provided a fixed reference for determining the separation point when both flow visualization fluid and tufts were used.

Both models were modified slightly after initial tests indicated a laminar boundary layer was present. Due to the relatively short characteristic length, the Reynolds number was too low for a supercritical flow condition. To trip the boundary layer, a 0.5 in. (1.27 cm) wide trip strip was applied to both models. After experimenting with various widths and locations, a 0.5 in. (1.27 cm) wide strip of double stick tape was applied just after the 30 deg pressure tap on the cylinder model and at a symmetric location on the underside of the cylinder. Number 70 grit silicon carbide granules were then sprinkled onto the tape and pressed into place. For the airfoil, the double stick tape was wrapped symmetrically about the leading edge and Number 60 grit granules were applied.

Boundary Layer Probe

A boundary layer probe was constructed of 0.25 in. (0.64 cm) o.d. stock stainless steel tubing with a machined taper to 0.05 in. (1.27 mm) o.d. tubing. A small piece of 0.008 in. (0.20 mm) shim stock was placed in the end of the 0.05 in. tubing. The end of the probe and the shim stock were heated and flattened, creating a smooth uniform slot in the end of the probe. Heating the end of the probe prevented cracking, but also caused the shim stock to be annealed and flattened as well. The result was a flattened pitot probe with a slot width of 0.006 in. (0.15 mm). The bottom of the flattened pitot probe was filed to a thickness of 0.003 in. (0.076 mm) to allow the average slot height above the surface to be 0.006 in. (0.15 mm) when the probe

was placed in contact with the models. The boundary layer probe is shown in Figure 8 above the airfoil model.

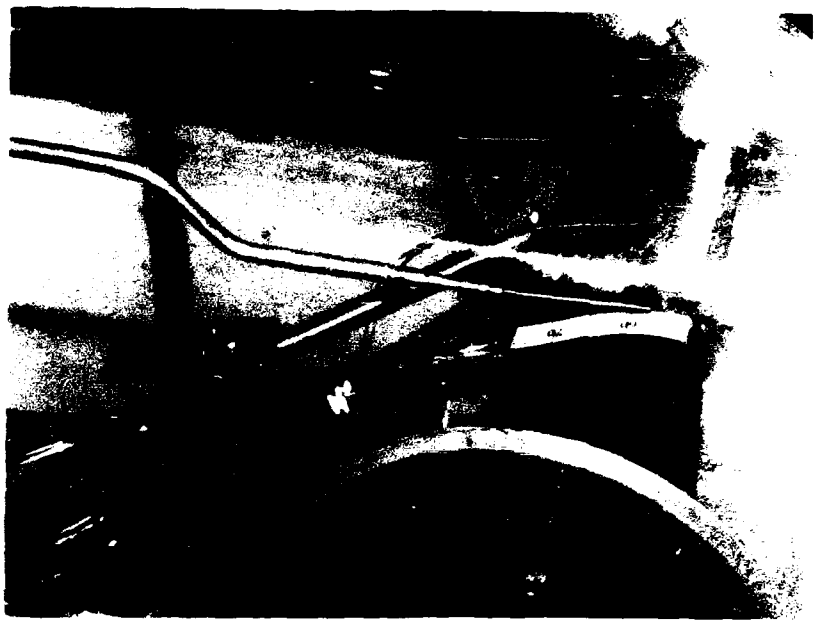

Fig. 8. Boundary Layer Probe

Riblets

The riblet material applied to both the cylinder and the airfoil models was Scotchcal™ Brand NPE-266 Drag Reduction Tape. The riblets are symmetrical V-shaped grooves with a peak-to-valley height of 0.006 in. (0.15 mm) as shown in Figure 9. The drag reduction tape, produced by the 3M Corporation, is adhesive backed and has an average thickness of 0.007 in. (0.18 mm). The material is applied by first cutting the material to the desired size and peeling off the backing. The adhesive is then sprayed with a mixture of water and detergent (1 tablespoon detergent to 1 gallon H_2O) and the riblet material is applied to the surface. The water/detergent mixture and air bubbles

are worked out using a felt squeegee. The water/detergent mixture not only aids in removing air bubbles but allows the riblet material to be repositioned once it is applied.

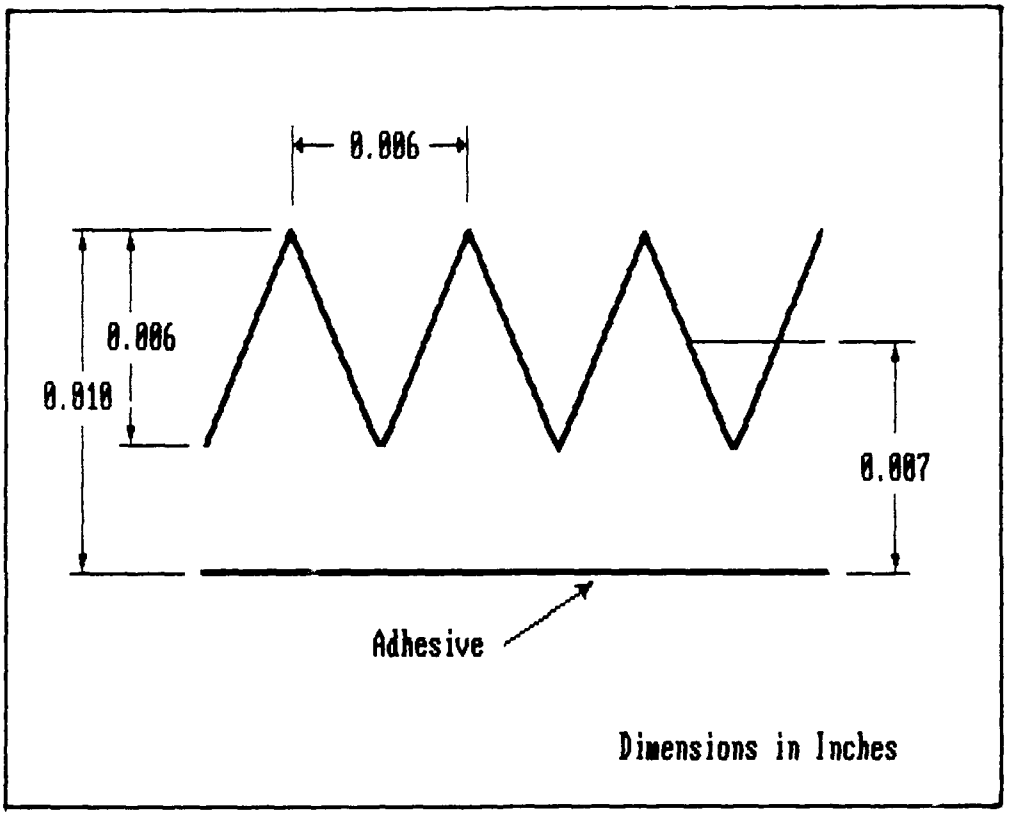

Fig. 9. Riblet Cross-Section

The riblet material was applied to both models beginning immediately behind the grit strip and extending all the way back to the trailing edge as shown in Figure 10. To retain full use of the pressure taps the riblets were applied in sections and butted up to the taps. As a result, the gap in the riblet material was kept to a minimum. For the cylinder this was essentially the width of the

pressure taps or approximately 0.05 in. (1.27 mm). Since the taps on the airfoil model are staggered, the gap was slightly larger, having a width of approximately 0.20 in. (5.08 mm).

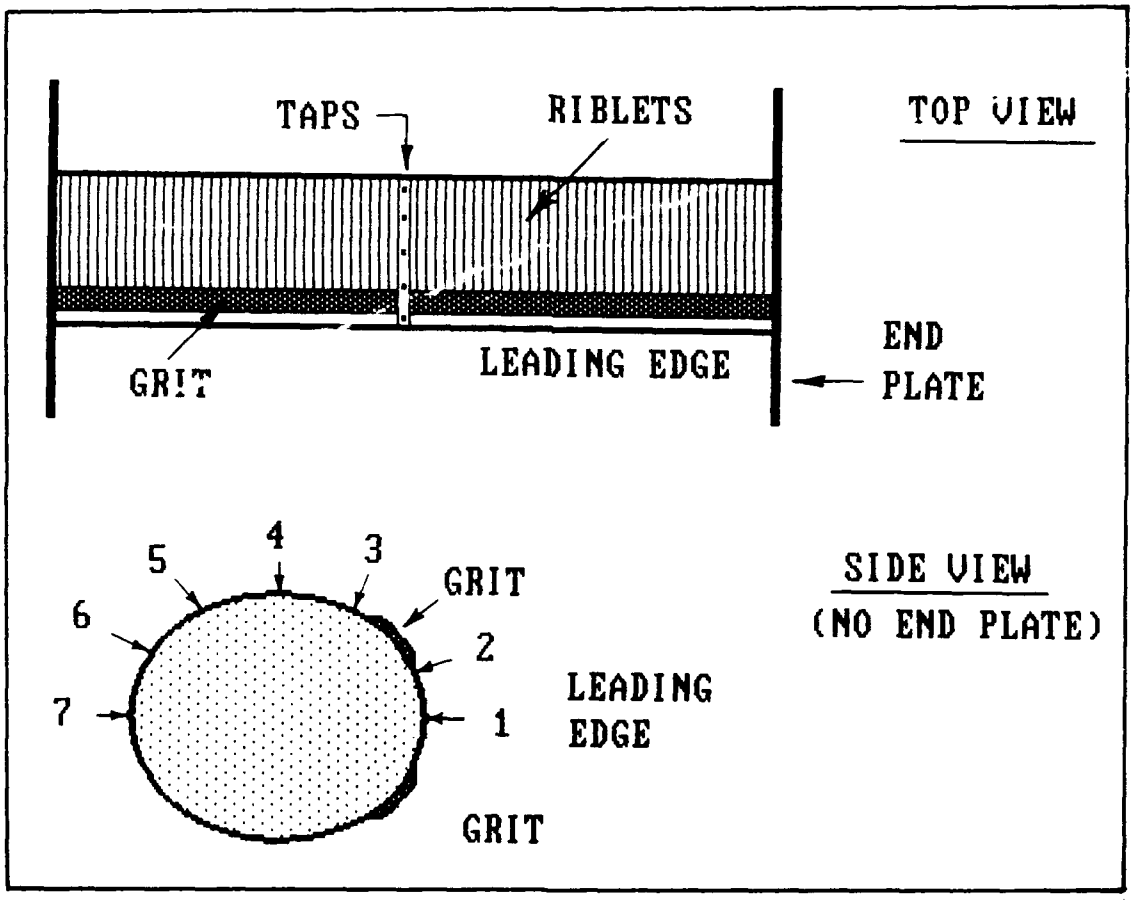

Fig. 10. Diagram of Cylinder Model with Riblets

IV. Experimental Procedure

The experimental research for this thesis was conducted in two distinct phases. The first phase involved tests with the cylinder model and the second centered around the airfoil model. Because the experimental procedure for each model was nearly identical, the following steps apply to both phases of the experiment.

Model Alignment

For both the airfoil at 0 deg AOA and the cylinder it was essential to have the leading edge (tap #1 for the cylinder) coincident with the stagnation point. For the cylinder model this was done by setting the AOA to -15.0 deg, thus positioning tap #1 at -15.0 deg and tap #2 at +15.0 degrees. If the stagnation point were to lie exactly between tap #1 and tap #2 then a run of the tunnel should yield $P_{tap\ \#1}$ equal to $P_{tap\ \#2}$. The run was conducted and the AOA was adjusted until the two static pressures were equal. The AOA indicator read -11.0 deg, indicating that the stagnation point was +4.0 deg above the tunnel centerline as shown in Figure 11. To verify this result, the AOA was set to +4.0 deg (indicated) and flow visualization fluid (hereafter referred to as oil drops) was applied to both the upper and lower surfaces. With air on, the oil drops flowed back to the separation point. Separation for both the upper and lower surface occurred at a point equidistant from tap #1, confirming that the stagnation point and the leading edge were coincident when the AOA indicator read +4.0 degrees.

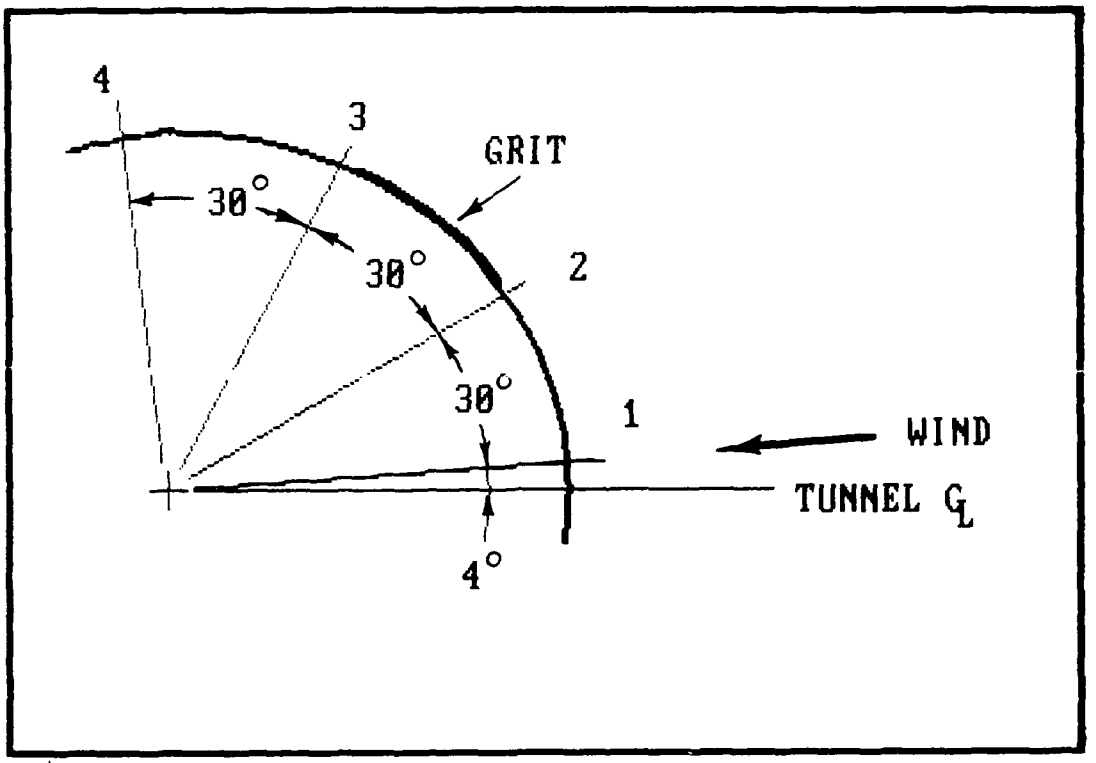

Fig. 11. Cylinder Model Alignment Diagram

The NACA 64_4-021 airfoil, like the cylinder, is symmetric about its centerline. Since the oil drop technique worked very effectively for aligning the cylinder model, the same technique was used to ensure the stagnation point occurred at the leading edge of the airfoil at 0 deg AOA. The separation location for the upper and lower surfaces was equidistant from the leading edge when the AOA indicator read +3.4 degrees.

Using the oil drop technique to align the models gave a preview of the flow separation that would be studied in detail later in the experiment. In the case of the cylinder, the angle at which separation occurred, ϕ_{sep}, was at 75.2 deg for freestream velocities

ranging throughout the test regime. This separation location is very close to that expected for laminar flow separation. From experiments and various theories, for a circular cylinder in laminar flow, ϕ_{sep} ranges from 78.5 to 83 deg (White, 1974:323; Kuethe and Chow, 1976:375). For the airfoil, separation occurred shortly after the maximum thickness location (x/c = 35 percent), again for all freestream velocities in the test regime. Separation after the maximum thickness location, which is also the point of maximum local velocity and the start of an adverse pressure gradient, is indicative of laminar flow separation (Abbott and von Doenhoff, 1959:94). Since a turbulent boundary layer was a prerequisite for this experiment with riblets, the models were modified with a grit strip to trip the boundary layer. The grit strip is described in detail in the Experimental Apparatus section of this report.

Dynamic Pressure Calibration

For low-speed subsonic flow, the test section velocity can be computed from Bernoulli's equation, $P_t - P_s = 1/2\,\rho V^2$, where $P_t - P_s$ is the dynamic pressure (q) in the test section. The total pressure in the test section, P_t, was obtained using a Kiel probe mounted in the traversing mechanism. The probe was positioned with the tip flush with the leading edge of the model, but with the probe approximately halfway between the upper surface of the model and the upper wall. P_s is the static pressure in the test section and is equal to P_2. Since it was not possible to have the total pressure tube in the test section during most of the testing, it was necessary

to plot the dynamic pressure as a function of two convenient and always measureable quantities. The dynamic pressure, $P_t - P_2$, was plotted versus $P_1 - P_2$, where P_1 and P_2 are the static pressures in the low speed settling chamber and test section respectively. Both the dynamic pressure and $P_1 - P_2$ were divided by the atmospheric pressure to remove the atmospheric effects from the calibration. Separate calibrations were performed for the cylinder model and the airfoil at four different angles of attack. (See Figures 12 and 13). Similar calibrations have been carried out successfully in the 14-inch wind tunnel (Fisk, 1988:39). The calibrations were done with the model in place since the presence of the model causes "solid blocking" which reduces the area through which the air must flow (Pope and Harper, 1966:309).

Plain Model

In order to fully observe what effects the application of riblets may have on an aerodynamic body, baseline data for the unaltered model must be obtained. Consequently, significant changes in the separation location can be confirmed using boundary layer surveys and pressure distribution curves in addition to flow visualization techniques.

Pressure Distribution. Baseline pressure distribution data was obtained on both models. Using the pressure taps the local static pressure is measured. The pressure coefficient, C_p, can then be computed and plotted with respect to chordwise location to give the pressure distribution. The pressure coefficient is computed using the

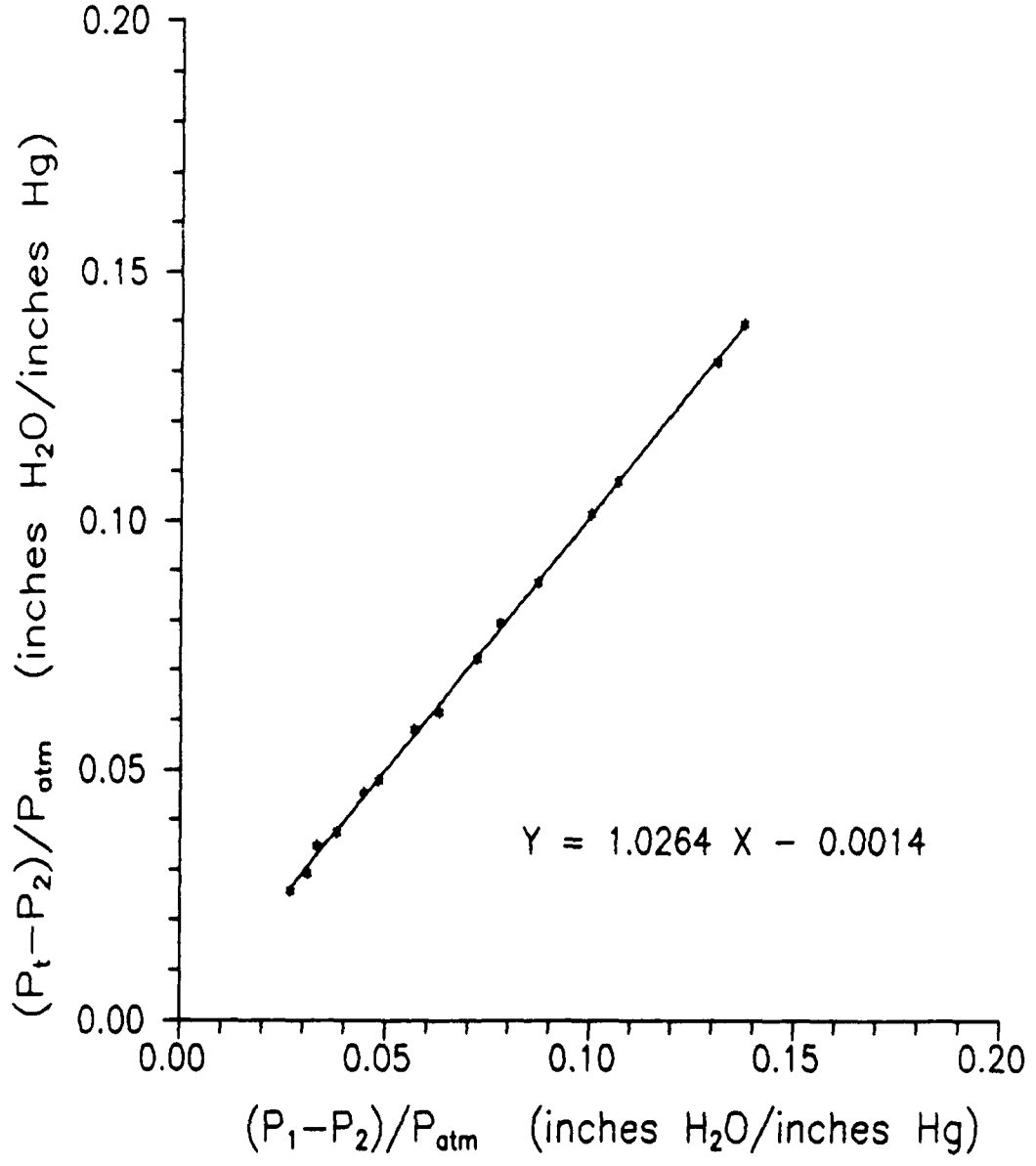

Fig. 12. Dynamic Pressure Calibration - Cylinder

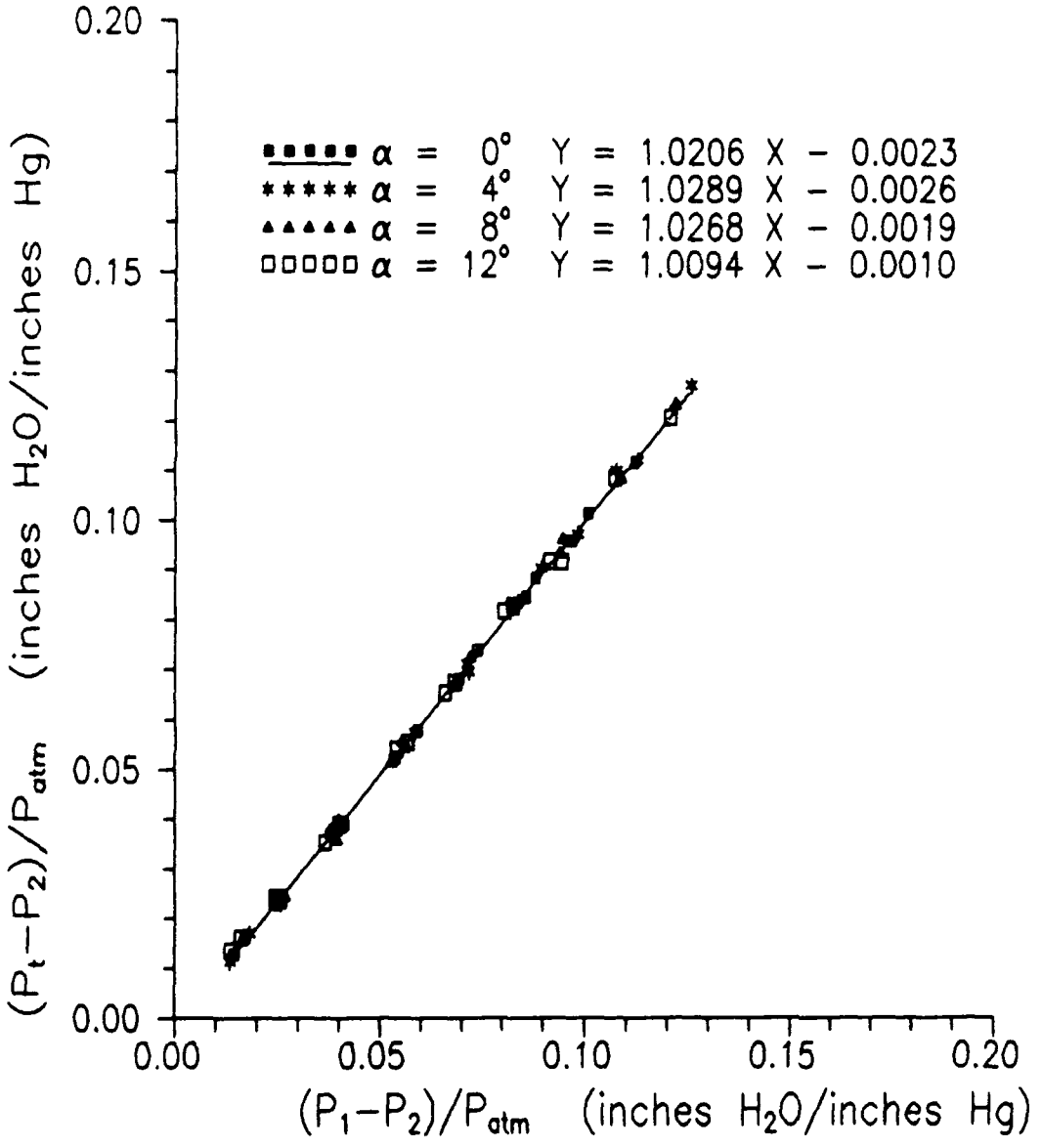

Fig. 13. Dynamic Pressure Calibration - Airfoil

equation, $C_p = (P_i - P_s)/q = (P_i - P_2)/q$, where P_i is the local static pressure (P_{tap}).

Boundary Layer Profile. Boundary layer profiles were an essential part of this experiment and were obtained for a number of different reasons. The first was to ensure that, after applying the trip strip, the boundary layer was in fact turbulent. By comparing a measured boundary layer profile with the Falkner-Skan laminar boundary layer solutions and the 1/7 Power Law for a turbulent boundary layer on a flat plate (Bertin and Smith, 1979:142,156) one can verify the existence of a turbulent boundary layer. A discussion of this procedure and the experimental results are presented in Appendix A.

The second purpose of boundary layer profiles was to provide data which could be used in determining the friction velocity, U_τ, which is needed to compute the non-dimensional riblet height, h^+. The friction velocity was computed using Cole's velocity-profile expression (Cebeci and Smith, 1974:123-124) as follows:

$$u^+ = \phi_1(y^+) + [\Pi(x)/\kappa]\, w(y/\delta) \qquad (9)$$

where

$u^+ = U/U_\tau$

U = flow velocity in the boundary layer at y (ft/sec)

$\phi_1(y^+) = (1/\kappa)\ln(y^+) + c$ where $y^+ = y\, U_\tau/\nu$ and $c = 5.0$

$\Pi(x)$ = Cole's profile parameter

κ = von Karman's mixing-length constant = 0.41

$w(y/\delta) = 2 \sin^2[(\pi/2)(y/\delta)]$

$\Pi(x)$ can be solved for if Equation 9 is evaluated at $y = \delta$, resulting in Equation 10:

$$U/U_\tau = (1/\kappa)\ln(yU_\tau/\nu) + c + [U_e/U_\tau - (1/\kappa)\ln(\delta U_\tau/\nu) - c] \sin^2[\pi y/(2\delta)] \quad (10)$$

There are two unknowns in Equation 10; U_τ and δ. All terms in Equation 10 are moved to the right hand side and set equal to an error parameter, ϵ. A value of δ is then assumed, and a range of U_τ is used for each point in the boundary layer profile, y and U, to produce a corresponding range of ϵ values for each data point in the boundary layer. Taking the square root of the sum of squares of ϵ produces a value proportional to the root-mean-square-error (ϵ_{rms}) for the chosen δ. Plotting ϵ_{rms} versus U_τ for each assumed δ results in a family of curves for which the minimum points of each curve can be connected to form a curve of minimum ϵ_{rms}. The minimum of this new curve gives the absolute minimum ϵ_{rms} and the corresponding δ and U_τ. Having solved for U_τ, the following equation can be used to solve for C_f, which is needed to calculate h^+ in Equation 7:

$$C_f = 2(U_\tau/U_e)^2 \quad (11)$$

The third reason for conducting a boundary layer survey is to verify separation. If a separation point has been identified using a flow visualization technique, such as oil drops or tufts, separation can be verified by comparing the measured boundary layer profile at

and in the vicinity of the point with the known separation profile as discussed in the Theory section on page 6.

Flow Visualization. Two different types of flow visualization techniques were used in this experiment; oil drops and tufts. For the plain models oil drops were used exclusively since the flow pattern very accurately indicated the separation point. The separation point determination using oil drops is considered, in most cases, to be within ± 0.02 in. (± 0.51 mm), based on repeatability and boundary layer profile verification. Since the oil drops worked so effectively for the plain model it was hoped that similar results could be obtained on the models with riblets. However, previous research involving separation in a diffuser found that oil drops are an ineffective flow visualization technique once riblets are applied (Martens, 1988:36). In preparation for similar problems with oil drops on riblets, a number of runs were made to correlate the behavior of tufts with the separation point indicated by the oil drops on the plain models.

The tufts were constructed of thin cotton fiber and attached at the end with 0.10 in. (2.54 mm) squares of Scotch brand adhesive tape. After experimenting with various tuft lengths, an exposed tuft length of 0.25 in. (0.635 cm) was found to be the optimum. Two different tuft configurations were tested; one with the tail of the tuft pointed upstream (hereafter referred to as forward-facing tufts) and the other with the tail pointed downstream (rear-facing tufts). The forward-facing tufts behaved as shown in Figure 14. For both the cylinder and the airfoil models, forward-facing tufts gave a strong indication of

attached flow upstream of the separation point and detached flow downstream of the separation point, but determination of the separation point was possible only within ± 0.05 in. (± 0.127 cm).

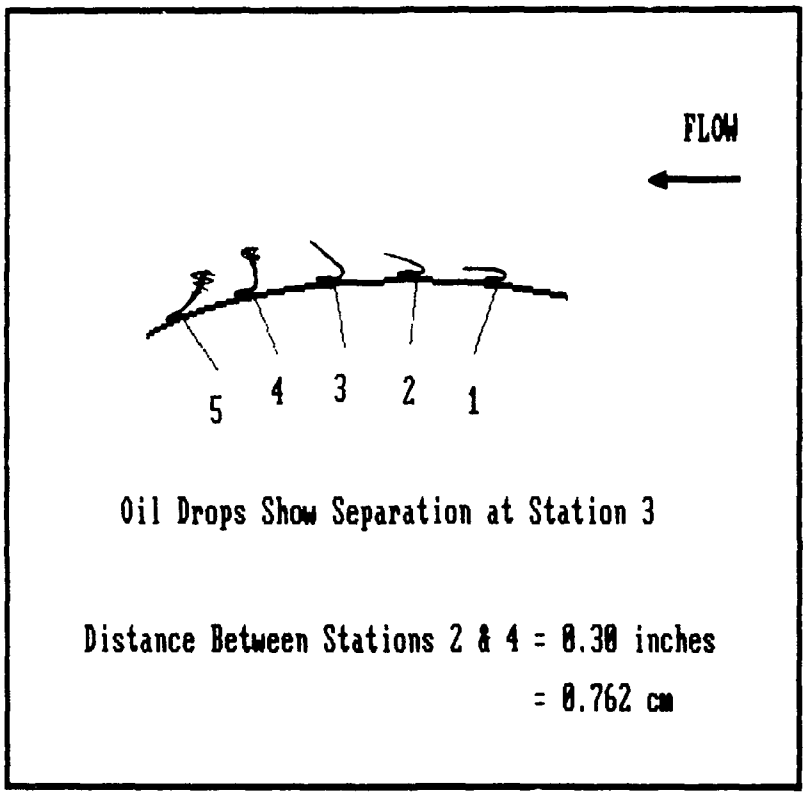

Fig. 14. Behavior of Forward-Facing Tufts

The rear-facing tufts, on the other hand, gave a more accurate indication of the separation point for the cylinder model. As shown in Figure 15, the tail of the rear-facing tufts did not begin to whip until the separation point was encountered. By using a number of tufts and by iterating with small variations in the tuft locations, the separation point was determined within ± 0.02 in. (± 0.051 cm) for

most airspeeds. On the airfoil model, however, the rear-facing tufts did not work well at all. The strong indication of separation that accompanied the rear-facing tufts on the cylinder model was not at all evident with the airfoil. Rear-facing tufts that were well behind the separation point, as shown by the oil drops and the forward-facing tufts, just laid along the surface and did not exhibit the strong whipping action as depicted in Figure 15. As a result, forward-facing tufts were used and the best determination of the separation point on the airfoil with riblets is within ± 0.05 in. (± 0.127 cm).

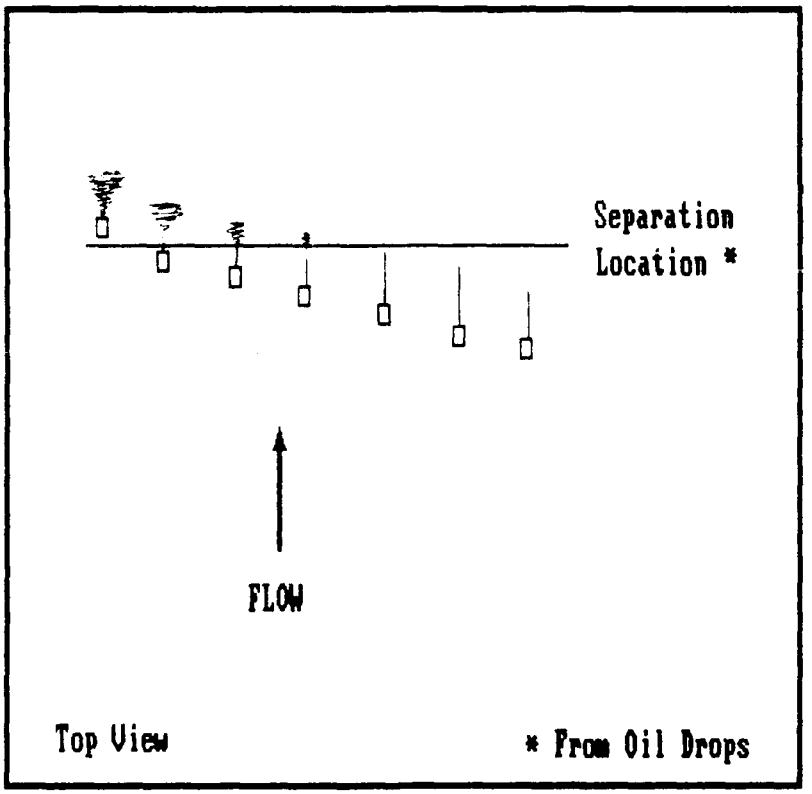

Fig. 15. Behavior of Rear-Facing Tufts

Model With Added Thickness

The question raised early in this investigation was whether any delay in separation, achieved by adding riblets, may be attributed to the modification of the model strictly by the added thickness. To answer this question the cylinder model was modified by adding a layer of transparency film and a paper backing which had a combined height of 0.007 in. (0.178 mm), the average height of the riblet material. The added thickness was placed exactly where the riblet material would eventually be attached, right behind the grit trip strip. A number of runs using oil drops revealed that the added thickness did not favorably affect the separation point. In fact, there was a slight reduction in the separation point ($2 < \Delta\phi_{sep} < 3$ deg) for the entire range of velocities tested. One possible reason for the reduction in ϕ_{sep} for the added thickness case is the reduced effectiveness of the boundary layer trip associated with butting the added thickness to the downstream edge of the grit strip.

NACA 64_4-021 is by definition a symmetric airfoil having a thickness to chord ratio of 21 per cent. Adding the riblet material to both sides of the airfoil raises the t/c ratio to only 21.6 percent. Due to the very definitive results from the cylinder, the small change in the airfoil shape, and the time constraints associated with this project, the airfoil was not tested with added thickness only.

Model With Riblets

After application of the riblet material, as described in the Experimental Apparatus section, it was necessary to repeat the steps

done for the plain models. Collecting the pressure distribution was a straightforward repeat of the plain model case. The results on the pressure distribution are very repeatable and individual C_p values are considered accurate to within ± 0.03.

As indicated when discussing flow visualization techniques, previous research involving separation in a diffuser found oil drops to be an ineffective technique on a surface with riblets. Unfortunately, this researcher has come to a similar conclusion. When the oil drops are applied to a smooth model, the surface tension of the droplet holds it together in its familiar circular shape until the flow velocity is sufficient to overcome the surface tension. In the case of the model with riblets, the riblets themselves destroy the surface tension of the droplet and act like capillary tubes, carrying the oil both upstream and downstream before the flow is even turned on. With the possibility of using oil drops dismissed, it was evident that tufts would need to be used once riblets were applied.

Determining the separation point using tufts was an iterative and time consuming endeavor. Even with painstaking care the separation point could be determined only within varying accuracies depending on the model and the airspeed. Appendix B contains the experimental data with the perceived accuracy on the separation point determination.

Once the separation point was identified, an attempt was made to verify the separation location by performing a boundary layer survey at and in the vicinity of the measured location. This was accomplished with results as discussed in the following section.

V. Results and Discussion

Cylinder

After initial model alignment and dynamic pressure calibration, the plain cylinder model was tested. Figure 16 shows the general configuration of the plain cylinder during the separation point investigation. (Note the 70 and 80 markings on the graph paper being used as a reference tape. They are not degree markings. The paper is labeled by tens in one inch increments and the label at the leading edge is 50). Looking down from above, as in Figure 17, a number of

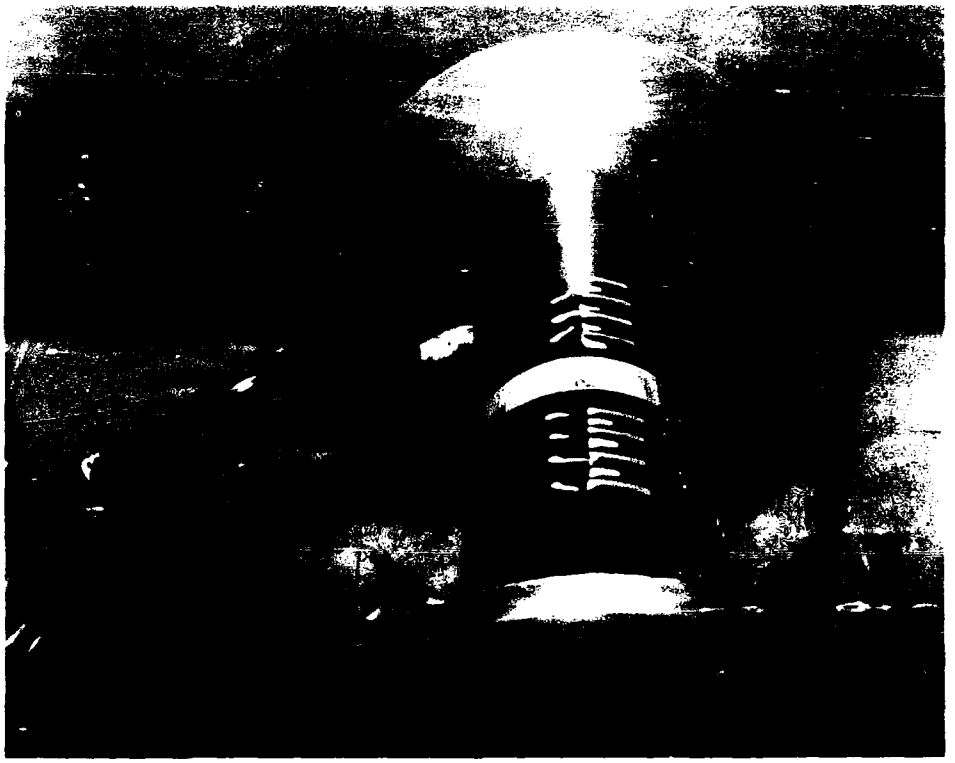

Fig. 16. Cylinder Model

observations can be made. First, span-wise flow is evident for distances greater than approximately 1.0 in. (2.54 cm) from the mid-span pressure taps. For this reason, the control area for all work done with the cylinder was limited to a distance of 1.0 in. from the taps, away from the reference tape, where the flow demonstrates two-dimensional behavior. Second, the oil drops ahead of the separation point flow back and define very nicely what appears to be the separation point. Third, oil drops behind the separation point flow forward and in some instances meet the downstream-flowing drops at the separation point.

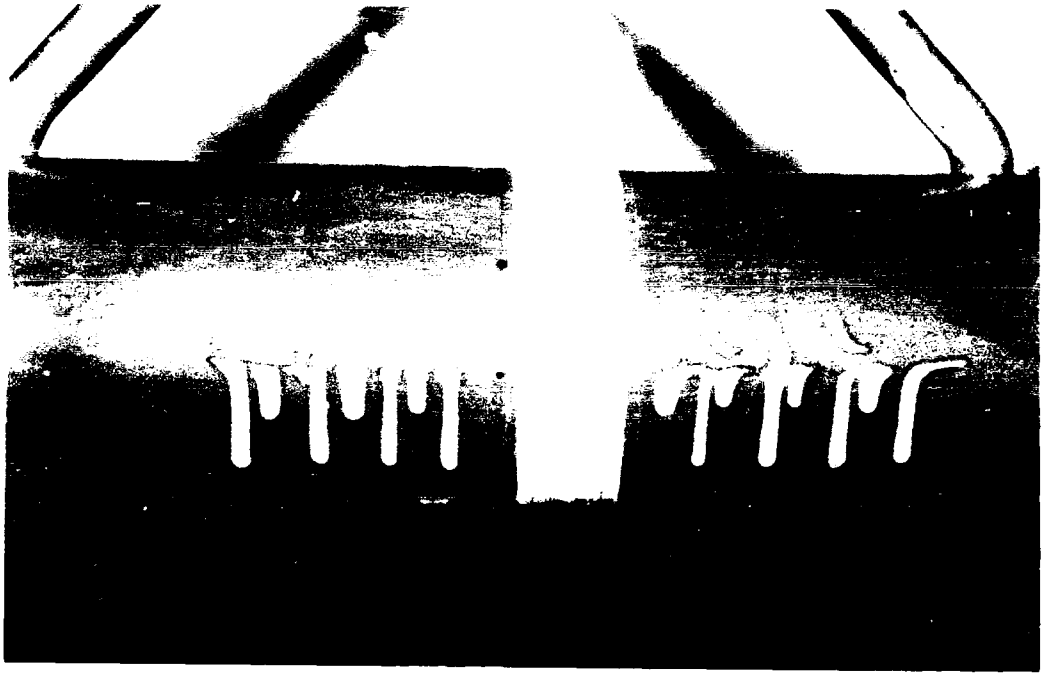

Fig. 17. Flow Visualization Fluid on the Cylinder

A boundary layer survey was accomplished at tap #3 (60 deg), not only for turbulent boundary layer verification as described in Appendix A, but also to determine the skin-friction coefficient at what eventually would be the leading edge of the riblets. Applying this data to Cole's law-of-the-wall, as described in Section IV, resulted in a U_τ of 6.85 ft/sec and a C_f of 0.00745. This value appeared to be somewhat high compared with skin-friction coefficients normally found in aerodynamic applications. This value of C_f was checked against that for a roughened flat plate since tap #3 was located only 0.10 in. (0.254 cm) downstream of the grit strip. The value of the local skin-friction coefficient for a roughened flat plate with the known local Reynolds number of 6.9×10^4 and an assumed nondimensional roughness height of 370 was found to be approximately 0.0079, nearly the same as that computed for the cylinder at tap #3 (Cebeci and Smith, 1974:198). This value of C_f was assumed to be constant over the range of velocities tested and could now be used in determining the nondimesional riblet height h^+, using Equation 11.

The results of the separation investigation using flow visualization techniques for the plain cylinder and the cylinder with riblets are presented in Figure 18. It should be noted that both methods of flow visualization for the cylinder are accurate only to within ± 0.02 in. (± 0.051 cm), which equates to ± 0.9 degree. The maximimum change in flow separation was 5.0 deg and occurred at an h^+ value of approximately 21 and a Reynolds number of 9.4×10^4. This represents a maximum delay in flow separation of 5.5 percent.

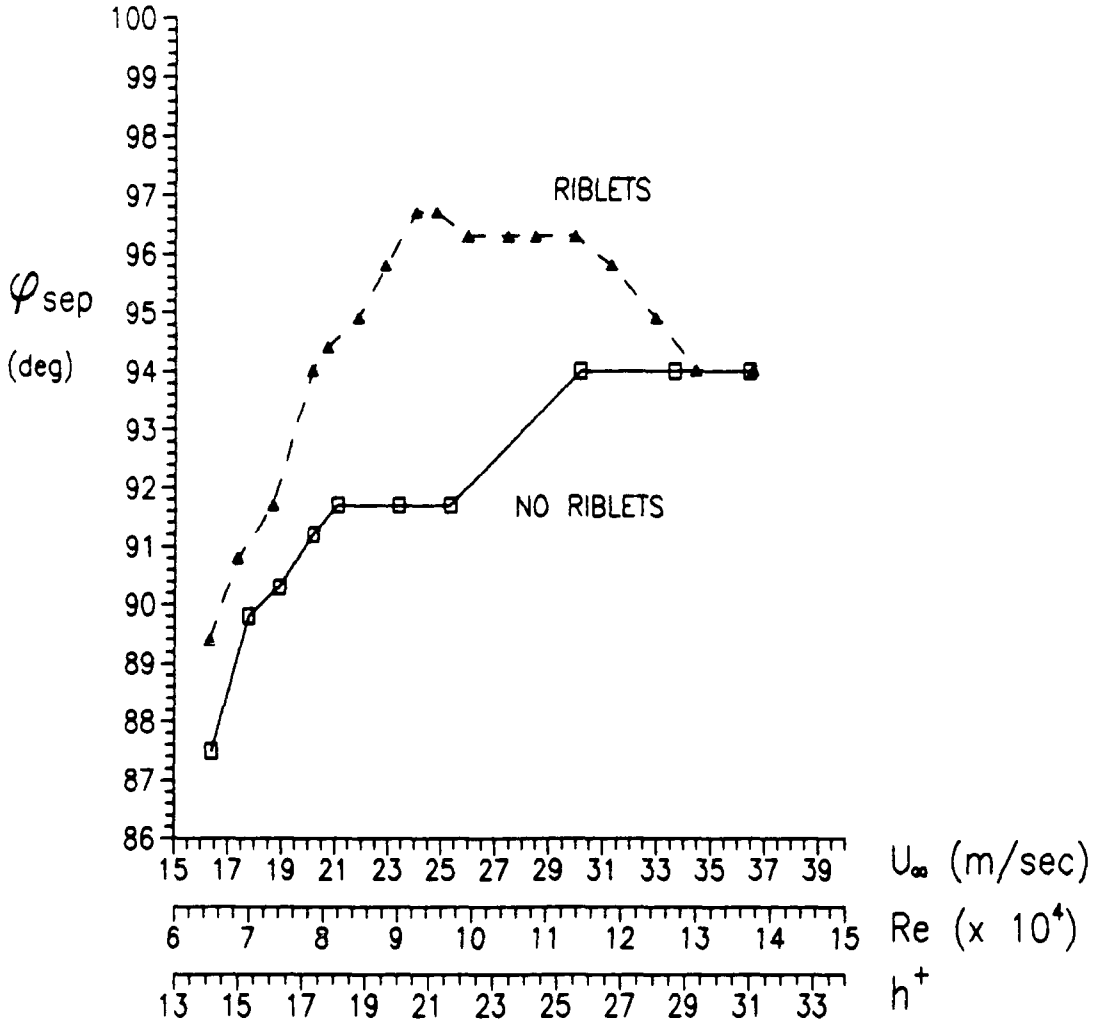

Fig. 18. Separation Locations for the Cylinder

Accurate results for freestream velocities less than 54 ft/sec (16.45 m/sec) could not be achieved since the condition of a turbulent boundary layer could not be satisfied even with the boundary layer trip.

Previous experiments to determine the separation point from a 2-D cylinder with a turbulent boundary layer have shown ϕ_{sep} to be about 100 deg (Kuethe and Chow, 1976:375). There are two possible explanations as to why the cylinder tested has a separation point 6 to

10 deg less than expected. The first is that the relatively close proximity of the test section walls to the model may be inducing some pressure effects and consequently degrading the 2-D flow assumption. The second explanation is that the testing is occuring under psuedo-supercritical conditions. For example, without the grit trip strip, the flow would be laminar and a subcritical flow condition would exist. By tripping the boundary layer a turbulent flow condition is achieved, but the Reynolds number is not sufficient to drive the separation point back to the true supercritical ϕ_{sep} location of 100 degrees.

By turning to the pressure distribution data an attempt can be made to verify and explain the delay in flow separation indicated by the flow visualization techniques. Figure 19 shows the pressure distribution curves for both model configurations at two different Reynolds numbers. Comparing the riblet and no riblet cases, the pressure is consistently higher at the 90 deg location on the cylinder for the riblet case and lower at the 120, 150, and 180 deg locations. The overall effect is an apparent reduction in $dC_p/d\phi$ for the region beginning at 60 deg and extending back to the trailing edge for the cylinder with riblets compared to the cylinder without riblets. It is possible that this apparent reduction in the adverse pressure gradient either contributes to or is responsible for the delay in flow separation.

An attempt to verify the separation point with a boundary layer survey did not prove convincing. The boundary layer profiles both with and without riblets are shown in Figure 20. From the two surveys

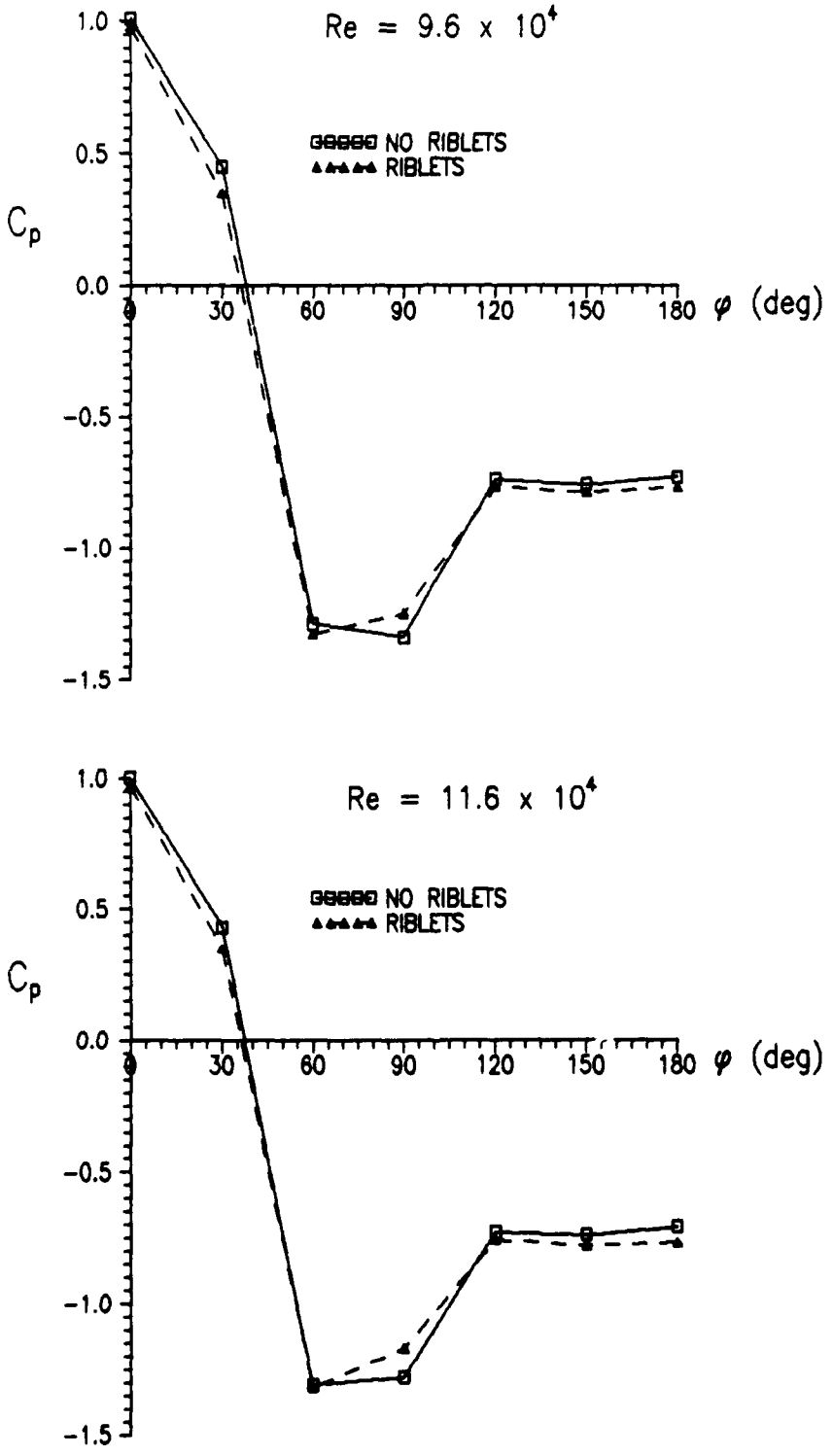

Fig. 19. Pressure Distributions on the Cylinder

done at 90 deg note the reduction in velocity for the riblet case at $y/\delta < 0.5$. While a reduction in the velocity gradient near the wall is an extension of the theory of reduced momentum transport near the surface caused by riblets, reduced velocities all the way out to $y/\delta = 0.5$ is unexpected and unexplained. Not visible in Figure 20 is the measured boundary layer thickness defined as the y for which $U = 0.99\ U_e$. The measured boundary layer thickness on the cylinder at $\phi = 90$ deg reduced from 0.060 in. (1.52 mm) for the no riblet case to 0.038 in. (0.965 mm) for the cylinder with riblets. It was theorized

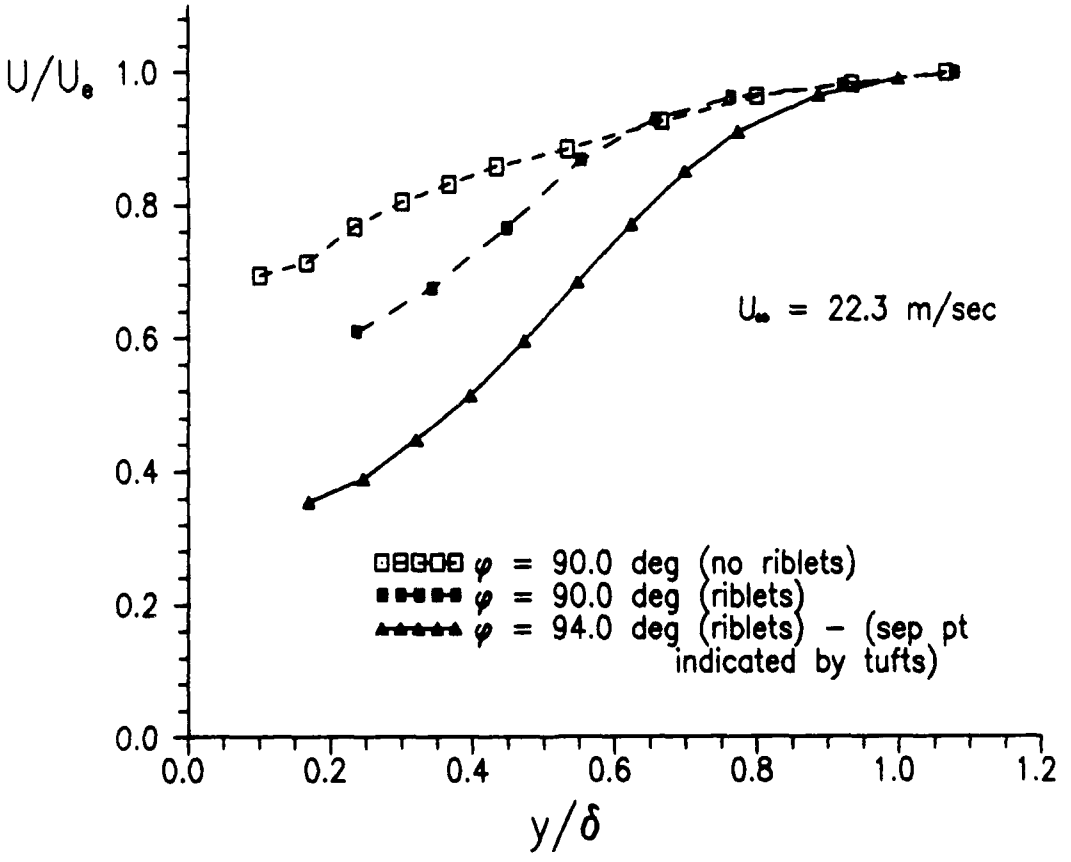

Fig. 20. Velocity Profile Comparison - Cylinder

that riblets retard the development of the turbulent boundary layer, but a reduction of over 30 percent in the boundary layer thickness was not anticipated.

Airfoil

The same procedure used with the cylinder was applied to the airfoil. Unlike the cylinder, however, the airfoil has an added parameter affecting separation, namely angle of attack. The airfoil was tested to investigate separation at 4 deg intervals beginning at 0 deg and continuing through 16 degrees. After the oil drop investigation of the separation point, however, three of the five configurations were eliminated. For both 0 and 4 deg, separation did not occur until the trailing edge as shown in Figure 21. For the case where α = 16 deg, separation occurred somewhere in the vicinity of the leading edge as shown in Figure 22. Since riblets could not delay the separation for any of these angles of attack, AOA's of only 8 and 12 deg were investigated.

Figure 23 shows the flow of oil drops over the airfoil at α = 8 deg. Immediately evident is the existence of secondary flow or vortices which are significantly reducing the area that can be considered two-dimensional. Further, the flow appears as if it is being accelerated, like subsonic flow through a convergent passage, in the only area even somewhat suited to be called the control area (approximately the center of the drops). The problem is even more severe at α = 12 deg, as seen in Figure 24. A possible reason for the severe vorticity was thought to be the presence of the mounting

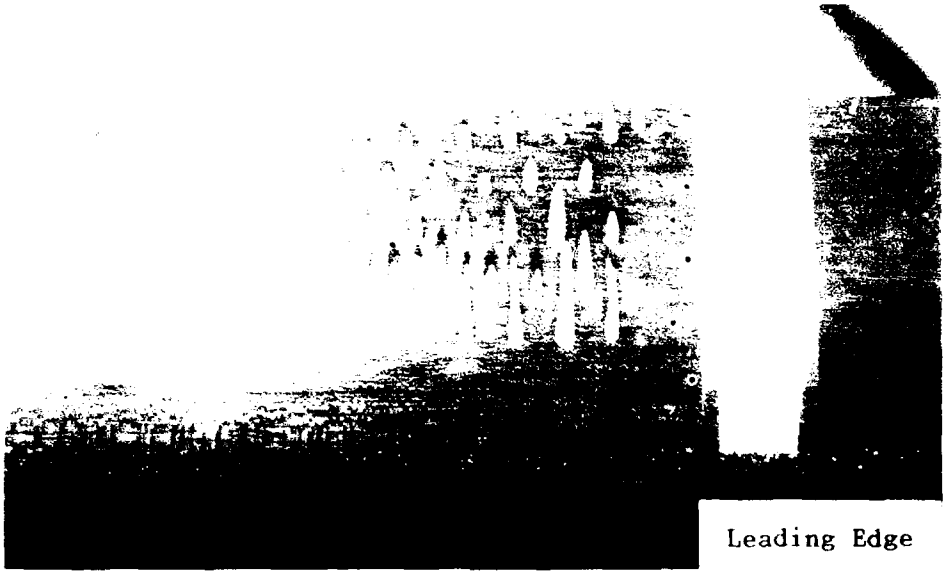

Fig. 21. Oil Drop Pattern when α = 0 deg and α = 4 deg

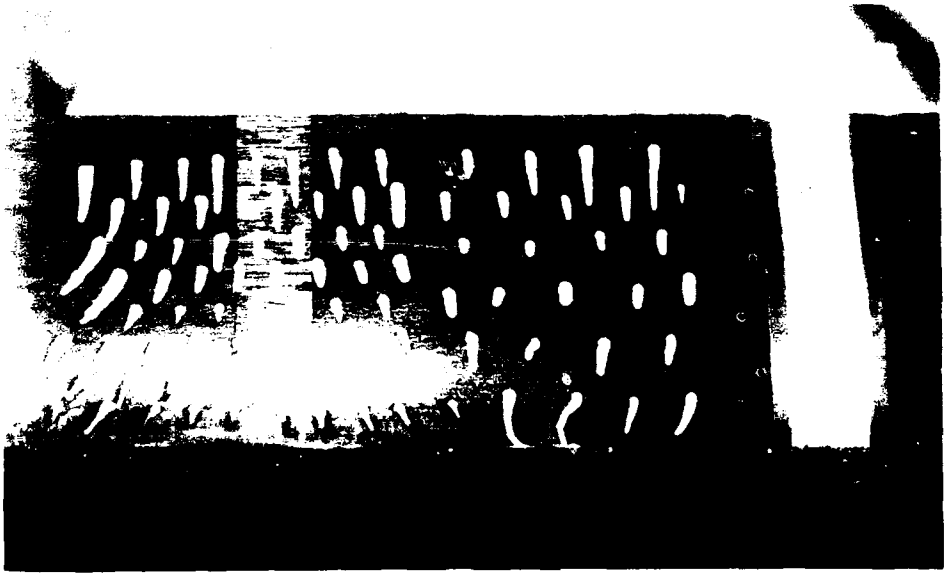

Fig. 22. Oil Drop Pattern when α = 16 deg

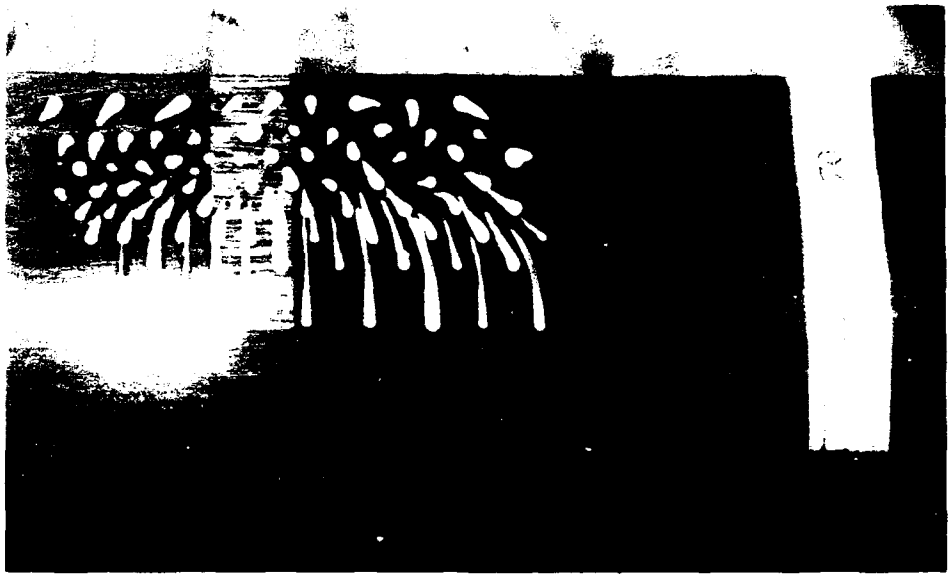

Fig. 23. Oil Drop Pattern when α = 8 deg

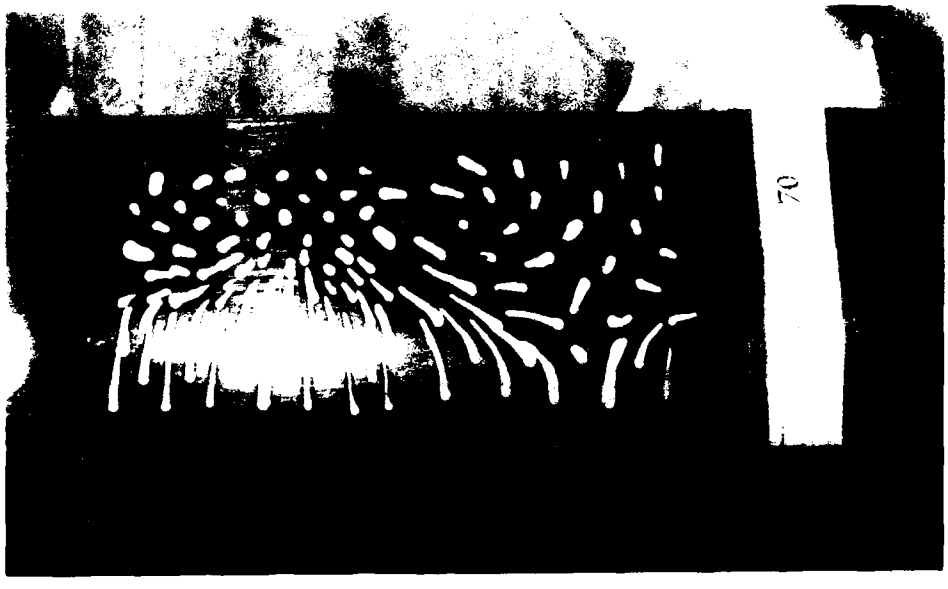

Fig. 24. Oil Drop Pattern when α = 12 deg

bracket. Removal of the bracket, however, did not alleviate this problem. Visible in Figure 24 are two somewhat distinct separation locations. The inboard separation point (close to taps) is at X_{sep} = 0.90 in. (2.286 cm), where X_{sep} is the distance from the leading edge to the separation point measured along the surface of the model. (Like the cylinder model, the decade markings on the reference tape are at one inch intervals and the grid mark of 50 is at the leading edge). The outboard separation point is at X_{sep} = 1.60 in. (4.064 cm). Since the location of the outboard separation point was taken as the control area for α = 8 deg, the same area was used for α = 12 deg with the exception that a very thin region was taken as the control area and extreme care was taken to make sure all flow visualization and boundary layer profiles took place within this region.

Separation points for the two angles of attack at various airspeeds was accomplished and the experimental data are recorded in Appendix B. Boundary layer surveys were accomplished to see whether the velocity distribution matched that of a separation profile. Figures 25 and 26 show the velocity profiles at one flow condition for points at and in the vicinity of the separation point indicated by the oil drops for α = 8 deg and α = 12 deg respectively. The velocity profiles for the airfoil support rather convincingly the location of the separation points determined by the oil drops. Note the inflection in the curve for boundary layer surveys downstream of the separation point. Boundary layer surveys were conducted upstream at tap #4 (X = 0.71 in.) to provide data for Cole's law-of-the-wall calculation of U_τ. For α = 8 deg, U_τ was found to be 6.7 ft/sec,

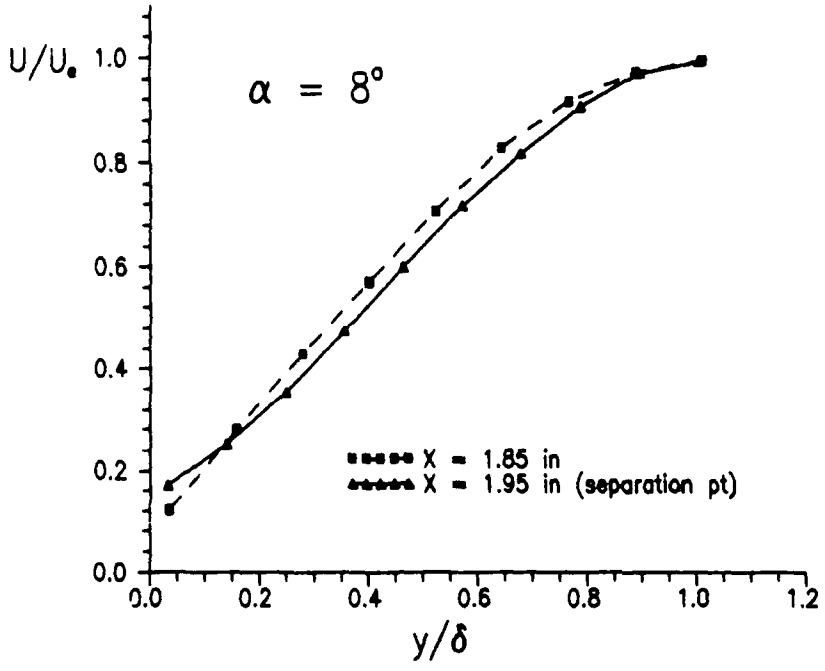

Fig. 25. Velocity Profiles (U_∞ = 32.9 m/sec)

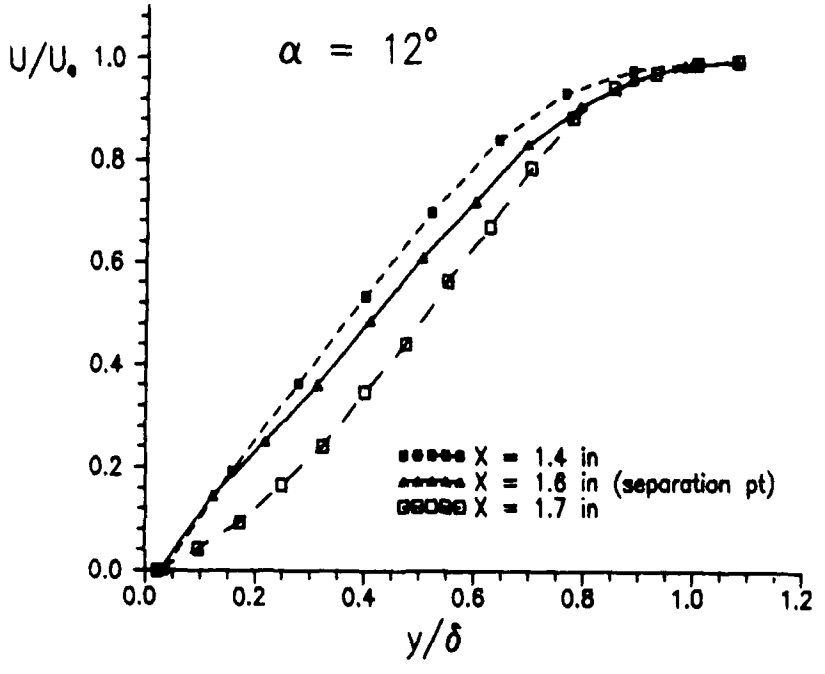

Fig. 26. Velocity Profiles (U_∞ = 27.4 m/sec)

corresponding to a C_f of 0.0076 from Equation 11. U_τ for α = 12 deg was 5.14 ft/sec, yielding a C_f of 0.0047. The computed C_f for both angles of attack was assumed to be constant over the range of velocities tested.

Riblets were applied to the model and the same tests were performed for the airfoil with riblets. The separation points for the riblet and no riblet cases are summarized in Figure 27. Note that the separation location along the surface, X_{sep}, has been divided by L,

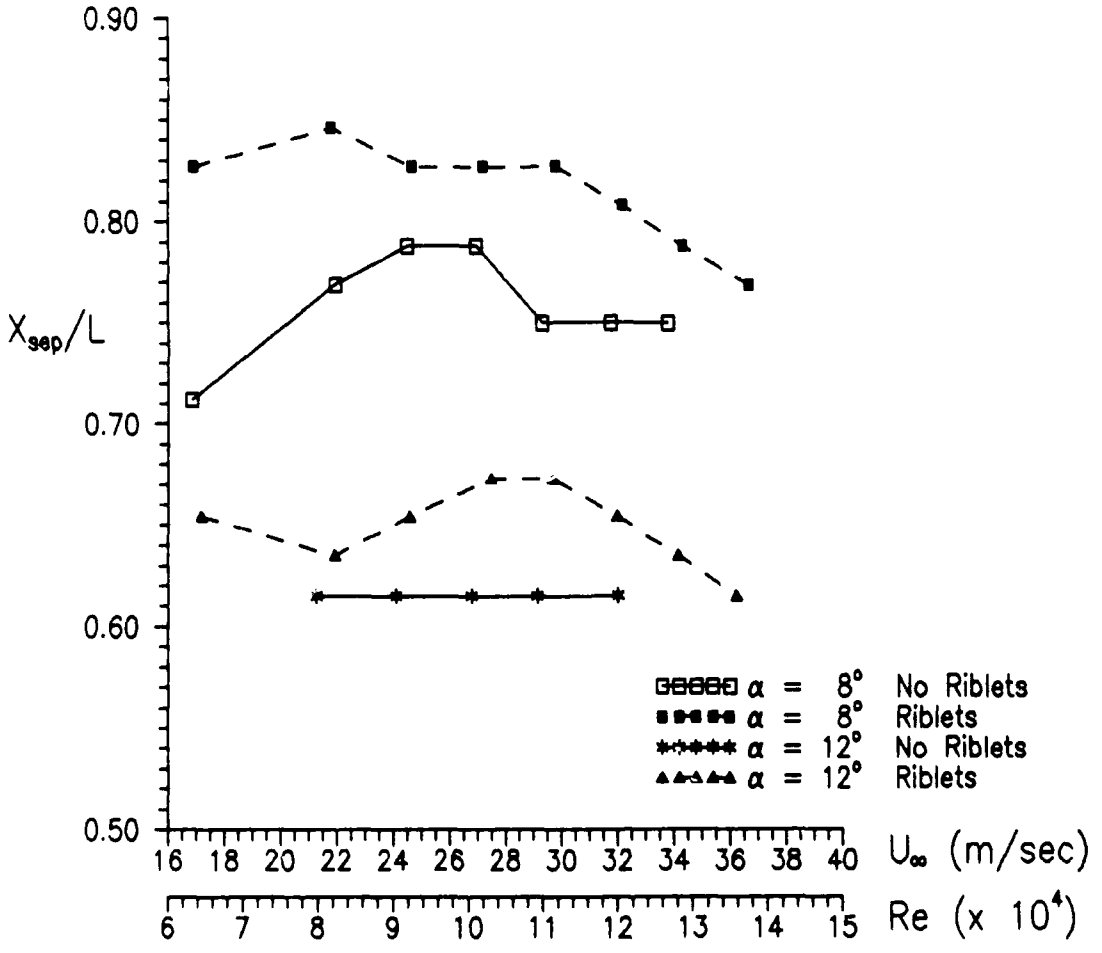

Fig. 27. Separation Locations for the Airfoil

the total surface distance from leading edge to trailing edge (L = 2.60 in.). As previously discussed the rear-facing tufts were not very effective for separation point determination on the airfoil. As a result, the accuracies generally varied between 0.05 and 0.10 in. (0.127 and 0.254 cm). This equates to X_{sep}/L errors of as much as ± 0.02 to ± 0.04. To observe how the separation point is affected by h^+, the α = 8 deg and α = 12 deg cases must be plotted separately in Figures 28 and 29 since C_f and consequently h^+ are not the same in both instances. However, due to the severe secondary flow effects and the relatively large inaccuracies resulting from the tuft visualization technique on the airfoil, high confidence in the riblet case was not achieved. Therefore, no conclusions relating values of

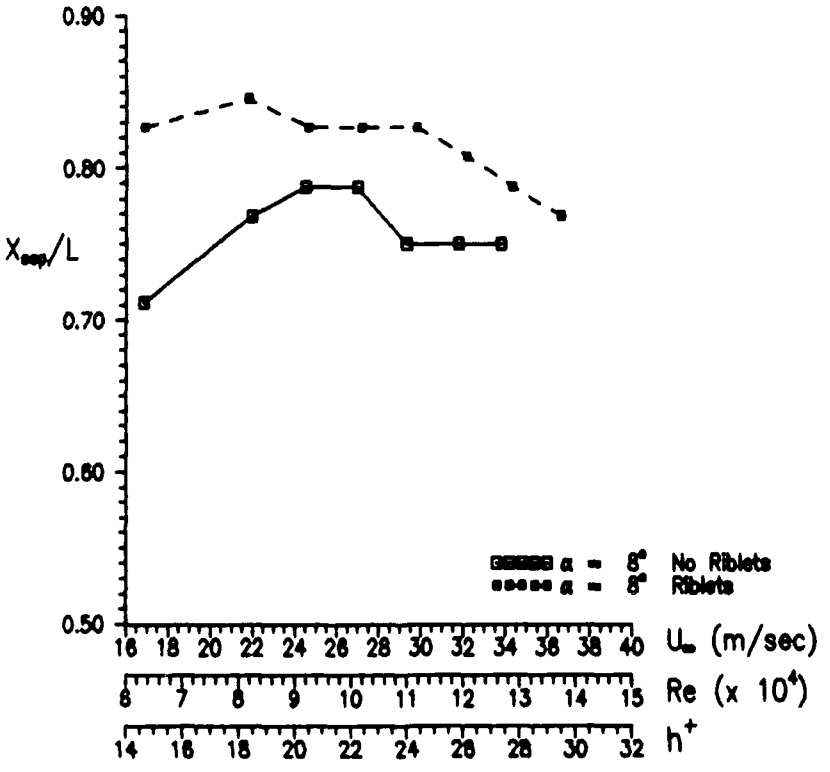

Pig. 28. Separation Locations for α = 8 deg

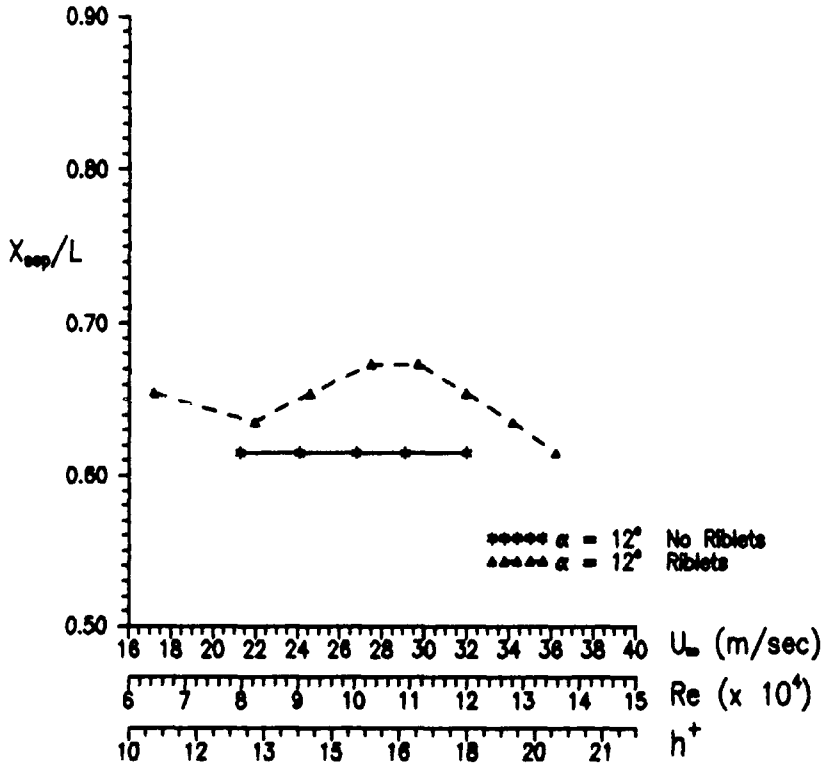

Fig. 29. Separation Locations for α = 12 deg

h^+ with maximum separation delay should be made. Complete flow separation data, including estimated accuracies on the flow visualization technique, are included in Appendix B.

Boundary layer surveys were performed at a few of the separation points indicated by the tufts. (The tuft indicated separation points are labeled in Figures 30-32). Figure 30 tends to indicate that for α = 8 deg, U_∞ = 33.8 m/sec, and h^+ = 27.5, the tuft technique erred on the optimistic side and that separation occurs ahead of the surveyed points as evidenced by the large inflection at y/δ = 0.3. Since the

accuracy for this tuft-determined separation point was noted as ± 0.10 in. (± 0.254 cm), it is conceivable that the separation point could be at 1.95 in. (4.95 cm), upstream of the surveyed points. In Figure 31 for α = 12 deg, U_∞ = 17 m/sec, and h^+ = 11.5, there appears to be good

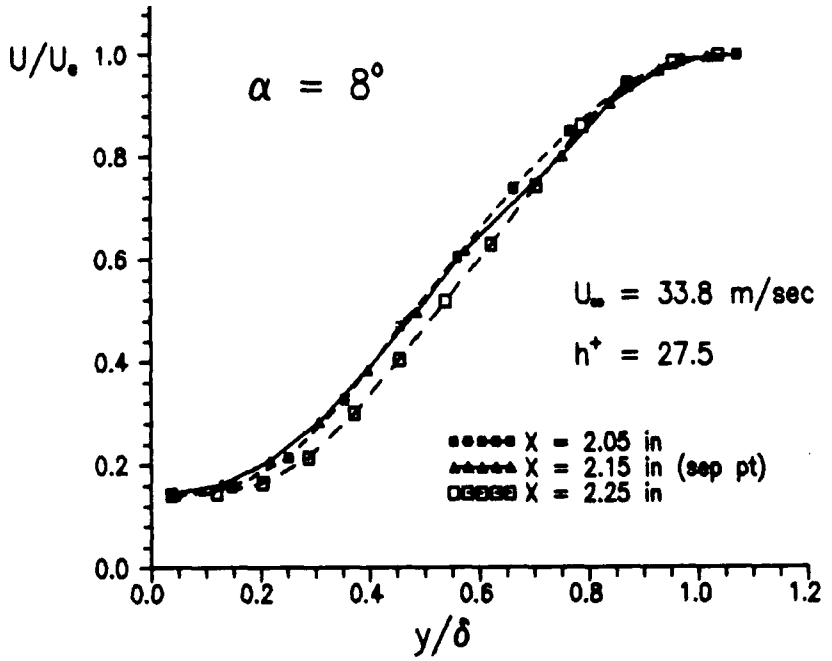

Fig. 30. Velocity Profiles

correlation between the velocity profile indication of separation and the tuft-determined separation point. Figure 32, however, once again indicates that separation has probably occurred upstream of the surveyed points.

The pressure distribution about the airfoil at 8 deg AOA is shown in Figure 33 for two Reynolds numbers and for both the riblet and no riblet cases. As in the case of the cylinder, the pressure distribution has been altered by the presence of riblets. Figure 34 shows similar plots for α = 12 deg.

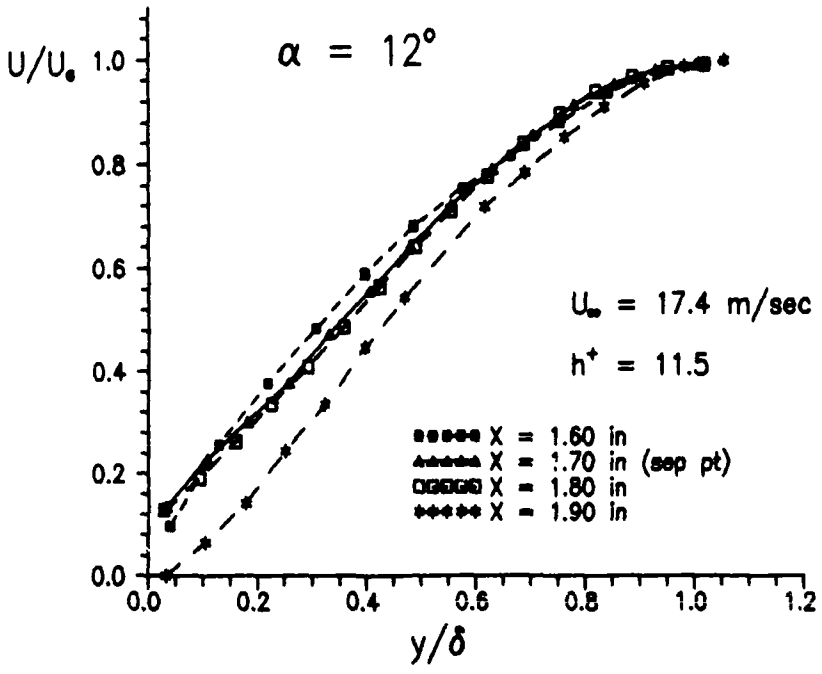

Fig. 31. Velocity Profiles

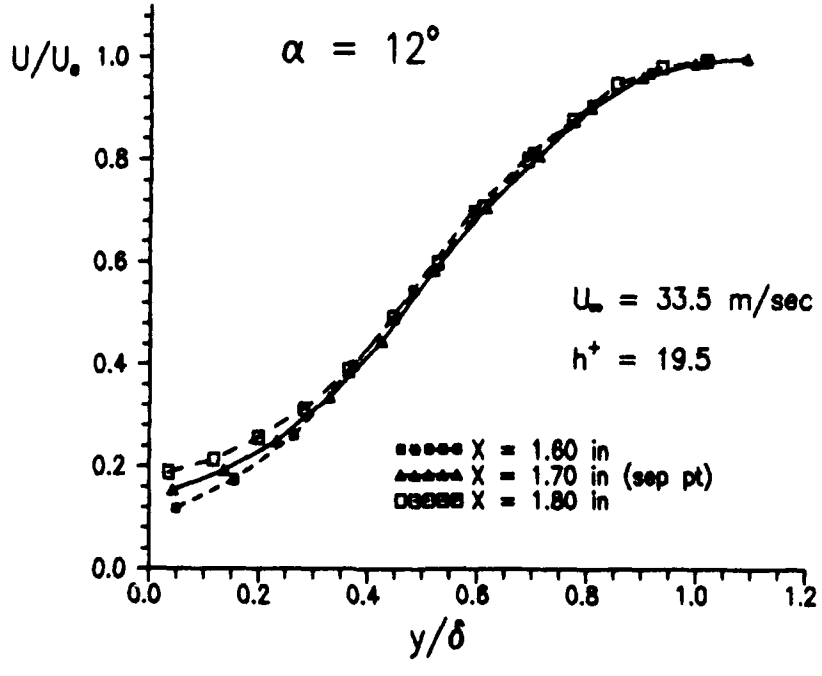

Fig. 32. Velocity Profiles

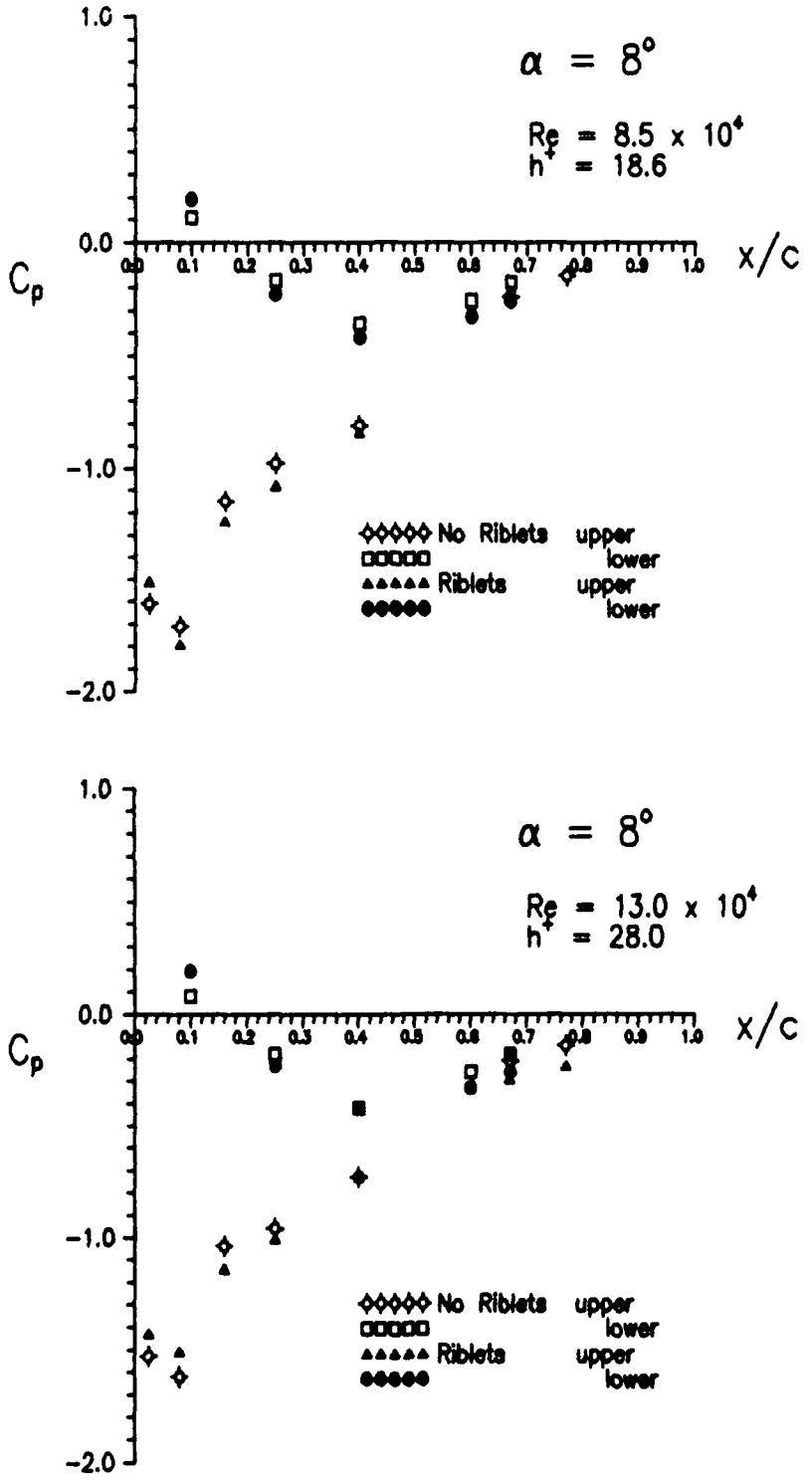

Fig. 33. Pressure Distributions on the Airfoil

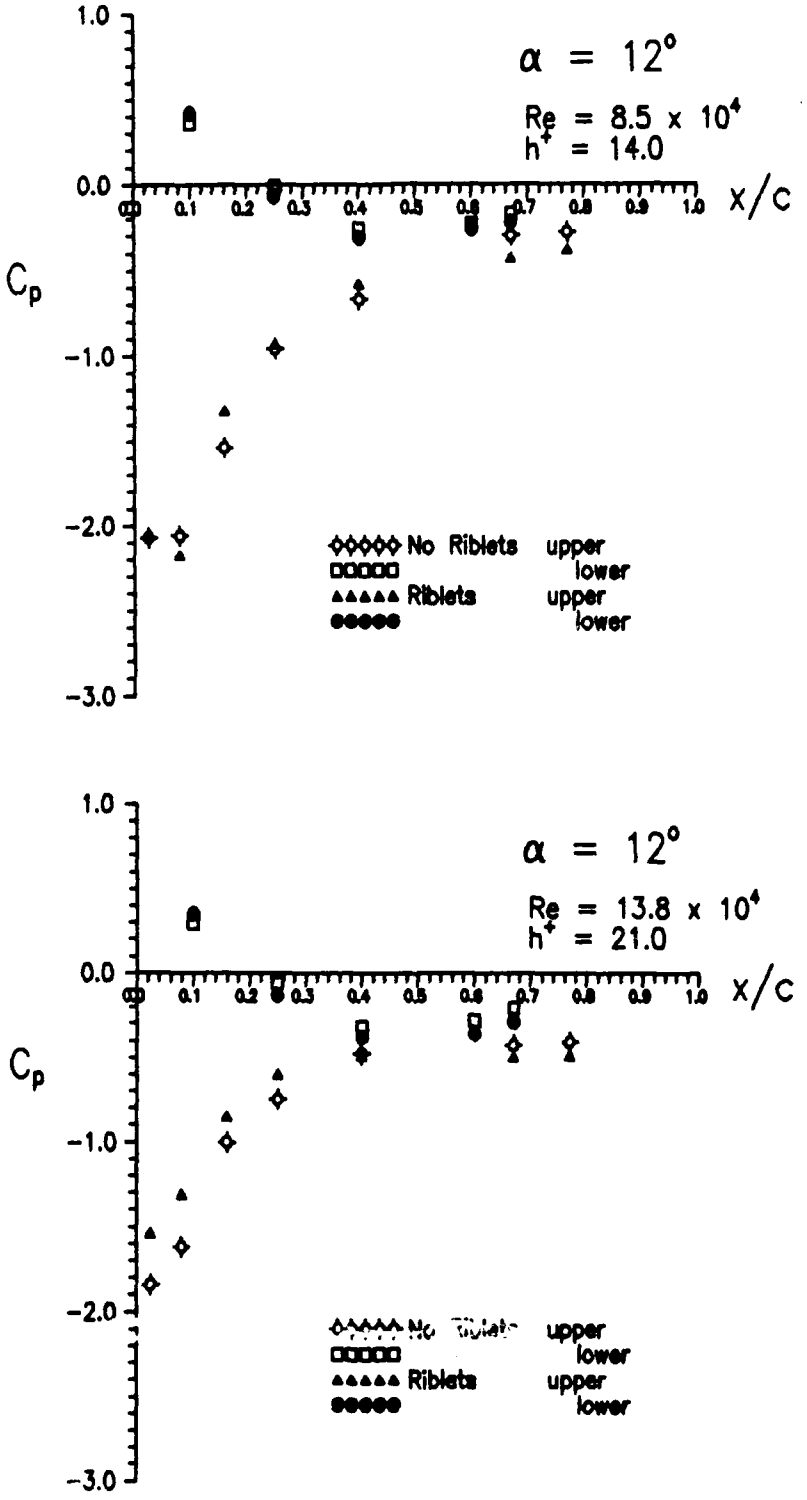

Fig. 34. Pressure Distributions on the Airfoil

Comparison to Diffuser

In light of the relatively meager delay in flow separation obtained on the airfoil and cylinder compared to the extreme delays experienced in the diffuser, a review of the diffuser experiment may be in order. Figure 35 is a drawing of the actual model used in the experiment and Figure 36 shows a side view of the model in the wind tunnel test section. For this arrangement, Martens derived the

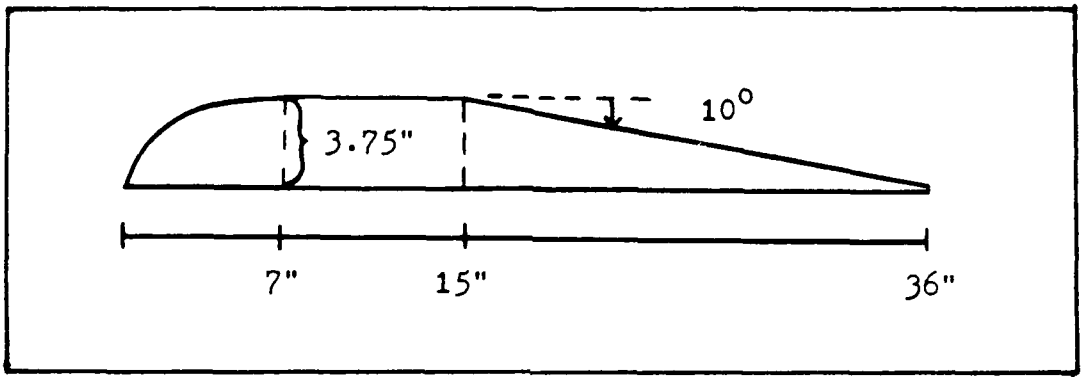

Fig. 35. Side View of the Diffuser Model

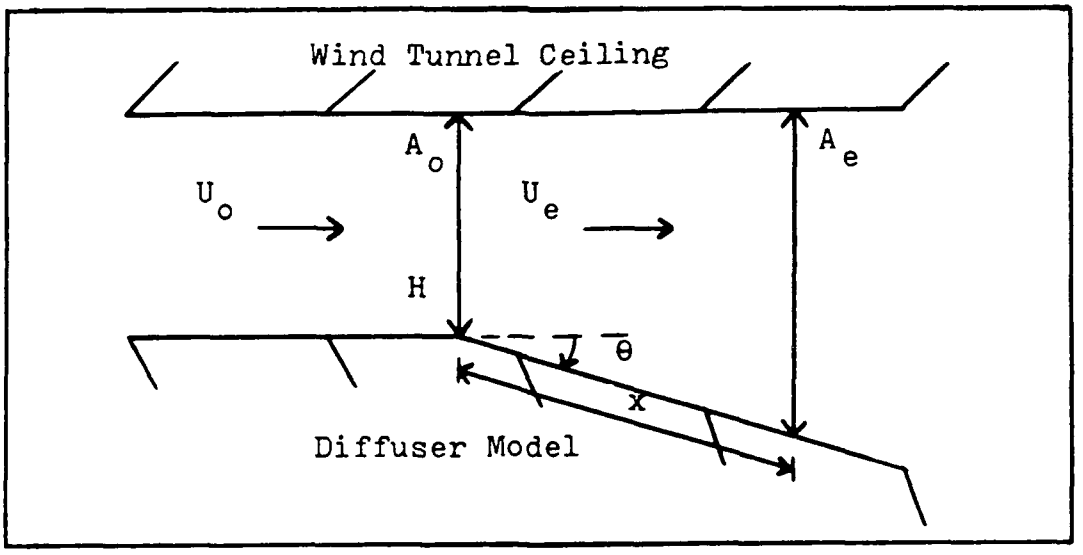

Fig. 36. Side View of the Diffuser Model in the Tunnel Test Section

following two expressions for the pressure coefficient and its rate of change with respect to X in the diffuser (Martens, 1988:84):

$$C_p = 1 - H^2/(H + X\tan\theta)^2$$

$$dC_p/dX = (2H^2\tan\theta)/(H + X\tan\theta)^3$$

Tables I and II contain the values of C_p and dC_p/dX at 1.0 in. (2.54 cm) intervals down the ramp of the diffuser. The throat height, H, is given in inches and the entries in Table II have the units of in^{-1}.

TABLE I

Computed Pressure Coefficient - Diffuser

		Cp			
	H (in.)	1.75	2.25	2.75	3.25
	0	0.0000	0.0000	0.0000	0.0000
	1	0.1747	0.1401	0.1169	0.1003
	2	0.3073	0.2526	0.2144	0.1862
	3	0.4104	0.3445	0.2966	0.2604
	4	0.4920	0.4204	0.3666	0.3248
	5	0.5578	0.4838	0.4266	0.3812
	6	0.6116	0.5374	0.4785	0.4309
	7	0.6561	0.5830	0.5236	0.4747
	8	0.6934	0.6222	0.5631	0.5137
	9	0.7250	0.6561	0.5979	0.5485
	10	0.7519	0.6857	0.6287	0.5797
X (in.)	11	0.7750	0.7116	0.6561	0.6078
	12	0.7951	0.7344	0.6806	0.6332
	13	0.8126	0.7546	0.7026	0.6561
	14	0.8279	0.7726	0.7223	0.6770
	15	0.8414	0.7887	0.7402	0.6960
	16	0.8534	0.8032	0.7564	0.7134
	17	0.8641	0.8162	0.7711	0.7294
	18	0.8737	0.8279	0.7845	0.7440
	19	0.8823	0.8386	0.7968	0.7575
	20	0.8900	0.8483	0.8080	0.7700
	21	0.8970	0.8571	0.8184	0.7815

The solid line in the columns represents the plain diffuser separation location for a throat velocity of 29.0 ft/sec and the dashed line represents the separation location with riblets applied. Note the magnitude of the dC_p/dX values. The highest value of the adverse pressure gradient is approximately 0.20/in. and exists over a very short distance. In the case of the cylinder or airfoil, however, the change in C_p may vary as much as 0.40 to 0.80 per inch. Based on the large delays in separation for the diffuser with riblets compared

TABLE II

Computed dC_p/dX for the Diffuser

		dCp/dX			
	H (in.)	1.75	2.25	2.75	3.25
	0	0.2015	0.1567	0.1282	0.1085
	1	0.1511	0.1250	0.1064	0.0926
	2	0.1162	0.1013	0.0893	0.0797
	3	0.0912	0.0832	0.0756	0.0690
	4	0.0730	0.0692	0.0646	0.0602
	5	0.0593	0.0581	0.0557	0.0528
	6	0.0488	0.0493	0.0483	0.0466
	7	0.0406	0.0422	0.0422	0.0413
	8	0.0342	0.0364	0.0370	0.0368
	9	0.0291	0.0316	0.0327	0.0329
	10	0.0249	0.0276	0.0290	0.0296
X (in.)	11	0.0215	0.0243	0.0259	0.0267
	12	0.0187	0.0215	0.0231	0.0241
	13	0.0164	0.0191	0.0208	0.0219
	14	0.0144	0.0170	0.0188	0.0199
	15	0.0127	0.0152	0.0170	0.0182
	16	0.0113	0.0137	0.0154	0.0166
	17	0.0101	0.0124	0.0140	0.0153
	18	0.0090	0.0112	0.0128	0.0141
	19	0.0081	0.0102	0.0117	0.0130
	20	0.0074	0.0093	0.0108	0.0120
	21	0.0067	0.0085	0.0099	0.0111

to the relatively small delay in separation caused by riblets on the cylinder and the airfoil, it appears that riblets are most effective in delaying flow separation in relatively weak adverse pressure gradients.

VI. Conclusions and Recommendations

Conclusions

Based on the investigation of the effect of riblets on separation from a cylinder and an airfoil in subsonic flow, the following conclusions are made:

1. The ability to accurately determine the separation point is considered good for the cylinder, fair for the airfoil at $\alpha = 8$ deg, and marginal for the airfoil at $\alpha = 12$ deg due to strong secondary flow that is affecting the 2-D nature of the model. For $h^+ < 30$ some delay in flow separation for the cylinder is realized. For the airfoil at both 8 and 12 deg angle of attack, a delay in separation is observed for the airfoil with riblets compared to the same model without riblets.

2. Riblets increase ϕ_{sep} by a maximum of 5.5 percent for the cylinder model. The maximum ϕ_{sep} is realized when $h^+ \approx 21$, which is nearly identical to that observed by Martens as the optimum h^+ in the diffuser. Strong secondary flow effects and inaccuracies with the tuft visualization technique on the airfoil prevent correlation of h^+ and maximum separation delay.

3. The application of riblets to the cylinder and the airfoil serves to alter the pressure distribution, possibly in such a manner as to reduce dC_p/dX upstream and in the vicinity of separation.

4. Riblets appear to be most effective in delaying flow separation in relatively weak adverse pressure gradients. Riblets

have very little effect in areas of large sustained adverse pressure gradients.

Recommendations

While this project showed limited success in delaying flow separation on a cylinder and an airfoil there are some areas that have yet to be addressed and some portions of this experiment that could be improved upon.

1. Since the pressure distribution around the aerodynamic bodies seemed to be consistently altered by the presence of riblets, it would be interesting to reinvestigate the diffuser, which is known to have significant delays in separation, to determine if the pressure distribution along the wall is undergoing a similar alteration in the C_p curve.

2. Confirm the data in this report and expand the body of knowledge on the airfoil by investigating more angles of attack, but more importantly, using models with a longer characteristic length. This should not only serve to increase the Reynolds number sufficiently to avoid boundary layer trips, but will also allow more accurate separation point determination. Use of a larger wind tunnel may eliminate or significantly reduce the secondary flow effects which hampered the airfoil experiment.

3. Boundary layer surveys proved to be fairly good indicators of flow separation if the boundary layer thickness was sufficiently large ($\delta > 0.10$ in.). Manual boundary layer surveys were too time consuming, however, to be used as the primary method of separation

determination. Use of a larger model, a boundary layer mouse, an analog-to-digital converter, and a microcomputer may automate the boundary layer survey technique to the point where it may be used as a primary indicator of flow separation. This would allow the same technique to be used for both the riblet and no riblet test cases.

A water table could be used to further investigate the effect of riblets on flow separation for a variety of models or diffuser geometries. Dye could be injected, possibly at numerous points along the model surface, to visually determine the separation point.

Bibliography

Abbott, Ira H. and Albert E. von Doenhoff. Theory of Wing Sections (Reprint Edition). New York: Dover Publications, 1959.

Bacher, E. V. and C. R. Smith. "Turbulent Boundary-Layer Modification by Surface Riblets," AIAA Journal, 24-8: 1382-1384 (August 1986).

Bertin, John J. and Michael L. Smith. Aerodynamics for Engineers. Englewood Cliffs NJ: Prentice-Hall, 1979.

Cebeci, Tuncer and A. M. O. Smith. Analysis of Turbulent Boundary Layers. New York: Academic Press, 1974.

Fisk, Capt Timothy E. Comparison of Split-Film and X-Film Measurements in 2-D Flow. MS Thesis, AFIT/GAE/AA/88D-16. School of Engineering, Air Force Institute of Technology (AU), Wright-Patterson AFB OH, December 1988.

Karamcheti, Krishnamurty. Principles of Ideal-Fluid Aerodynamics (Reprint Edition). Malabar FL: Robert E. Krieger Publishing Company, 1980.

Kuethe, Arnold M. and Chuen-Yen Chow. Foundations of Aerodynamics: Bases of Aerodynamic Design (Third Edition). New York: John Wiley & Sons, 1976.

Martens, Nathan W. Effect of Riblets Upon Flow Separation in a Subsonic Diffuser. MS Thesis, AFIT/GAE/AA/88D-23. School of Engineering, Air Force Institute of Technology (AU), Wright-Patterson AFB OH, December 1988.

Pope, Alan and John J. Harper. Low Speed Wind Tunnel Testing. New York: John Wiley & Sons, 1966.

Wallace, J. M. and J. L. Balint. "Viscous Drag Reduction Using Streamwise Aligned Riblets: Survey and New Results," Proceedings of the Turbulence Management and Relaminarisation IUTAM Symposium, edited by H. W. Liepmann and R. Narasimha: 133-147. Heidelberg West Germany: Springer-Verlag, 1988.

Walsh, M. J. "Turbulent Boundary Layer Drag Reduction Using Riblets," AIAA 20th Aerospace Sciences Meeting. Paper No. 82-0169. New York: American Institute of Aeronautics and Astronautics, 1982.

White, Frank M. Viscous Fluid Flow. New York: McGraw-Hill Book Company, 1974.

Appendix A: Turbulent Flow Verification

A prerequisite for this experiment was the existence of a turbulent boundary layer. Initial investigations of flow over both the cylinder and the airfoil models indicated that laminar flow was present over the entire test regime. Significant measures were taken to trip the boundary layer as discussed in Section III. To confirm that the boundary layer trip successfully induced turbulent flow, boundary layer surveys were performed and the corresponding velocity profiles were compared to theoretical laminar and turbulent profiles.

The nondimensional family of velocity profiles for the laminar boundary layer are shown in Figure 37. The solid line where $\beta = 0$ is the Blasius solution for flow over a flat plate. For flow in the presence of pressure gradients $\beta \neq 0$, but rather (Bertin and Smith, 1979:139-145):

$$\beta = (2s/U_e)(dU_e/ds) \tag{14}$$

where

$$s = \int U_e \, dX \tag{15}$$

Unlike the laminar case, the turbulent velocity profile is determined only by experiment and for flow over a flat plate is approximated by the 1/7 Power Law. The 1/7 Power Law is an experimental result which states simply that for a turbulent boundary layer over a flat plate:

$$U/U_e = (y/\delta)^{1/7} \tag{16}$$

where U is the time averaged velocity and δ is the boundary layer thickness defined as the y for which $U/U_e = 0.99$. The boundary layer surveys performed for turbulent flow verfication were done in the presence of pressure gradients, but the 1/7 Power Law is used as an approximation.

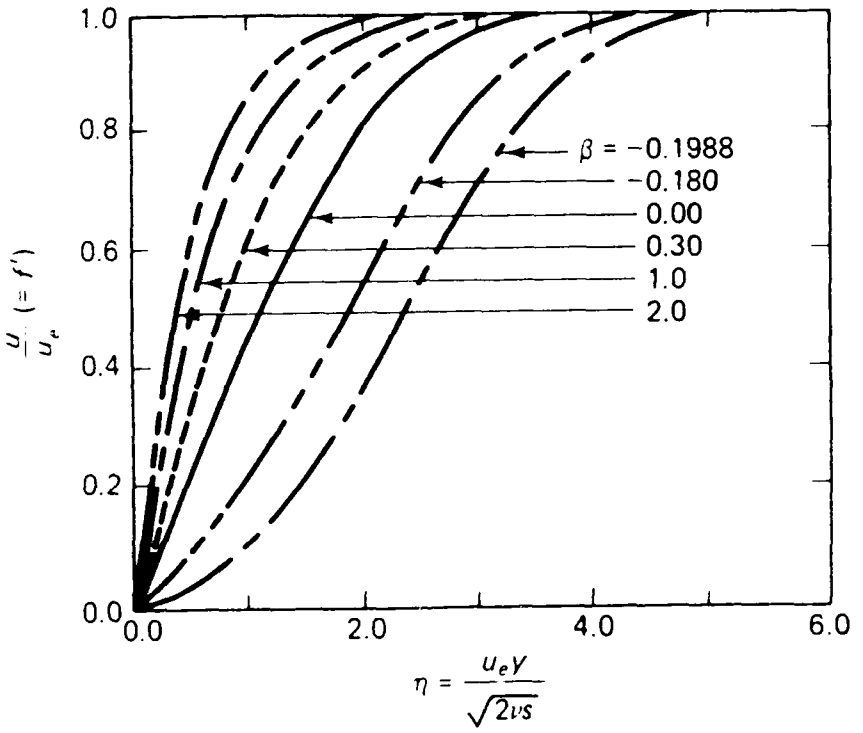

Fig. 37. Solutions for the Falkner-Skan, Laminar, Similarity Flows (Bertin and Smith, 1979:142)

Figure 38 shows the boundary layer velocity profile for the cylinder without riblets at ø = 60 deg compared to the laminar and approximate turbulent profiles and confirms the presence of turbulent flow over the clyinder.

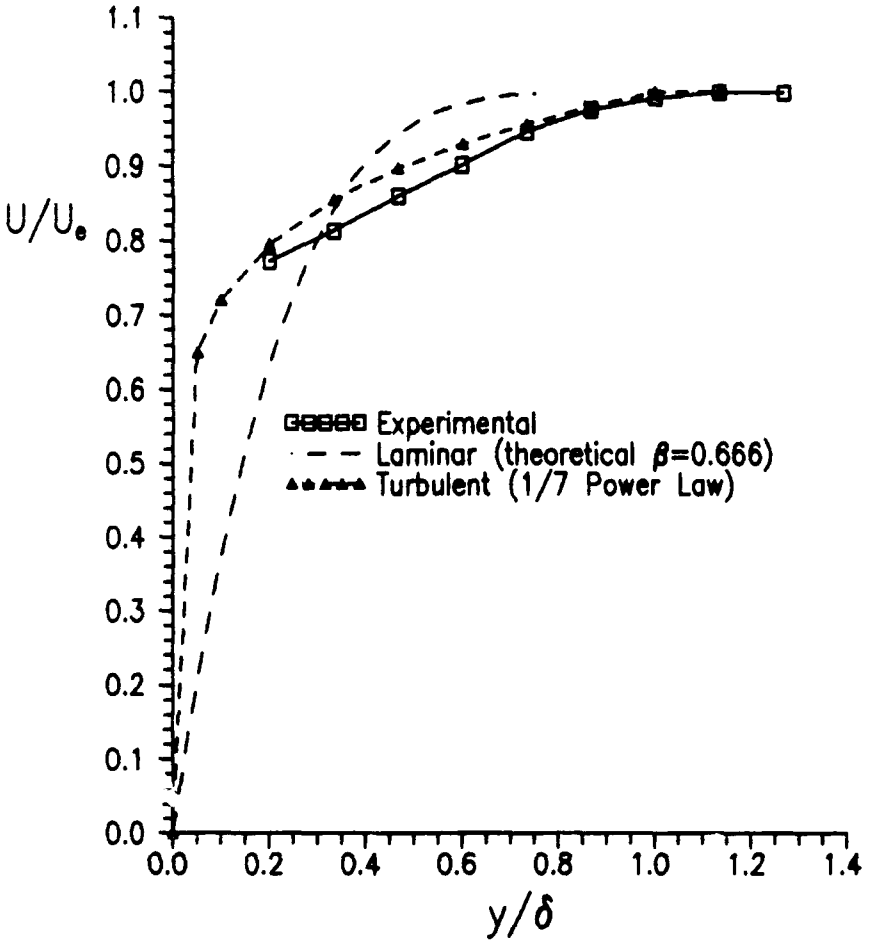

Fig. 38. Boundary Layer Velocity Profile for the Cylinder (ϕ = 60 deg and U_∞ = 79 ft/sec = 24 m/sec)

Figures 39 and 40 show the boundary layer velocity profiles for the airfoil at 8 and 12 deg AOA respectively, performed at the tap #4 chord location (x/c = 0.25). Note that the presence of an adverse pressure gradient has caused the measured profile in Figure 39 to deviate from the flat plate, 1/7 Power Law assumption. Nonetheless, the measured profiles for both 8 and 12 deg AOA show that the boundary layer has been successfully tripped so that a laminar flow condition no longer exists.

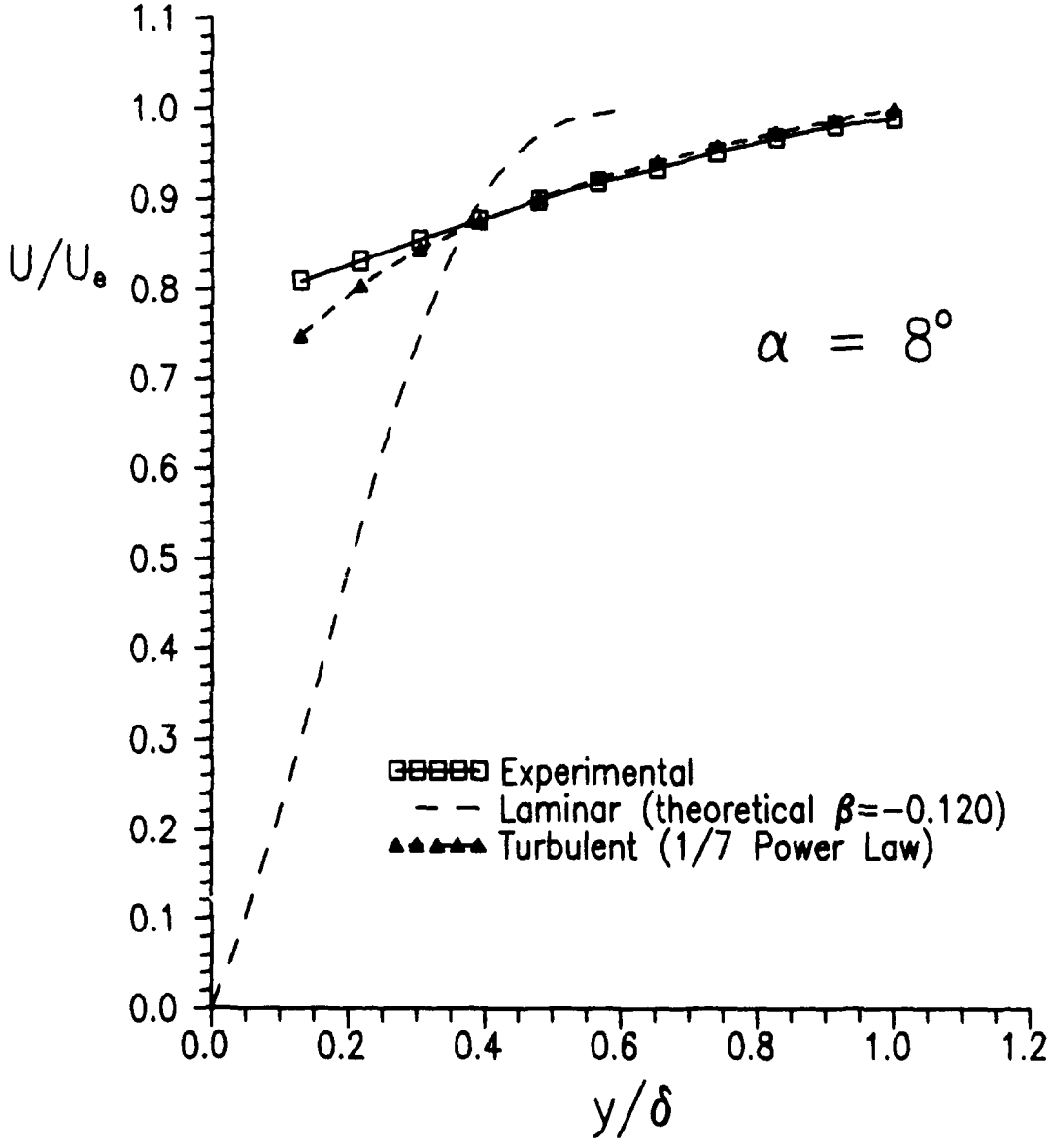

Fig. 39. Boundary Layer Profile (U_∞ = 81 ft/sec = 24.7 m/sec)

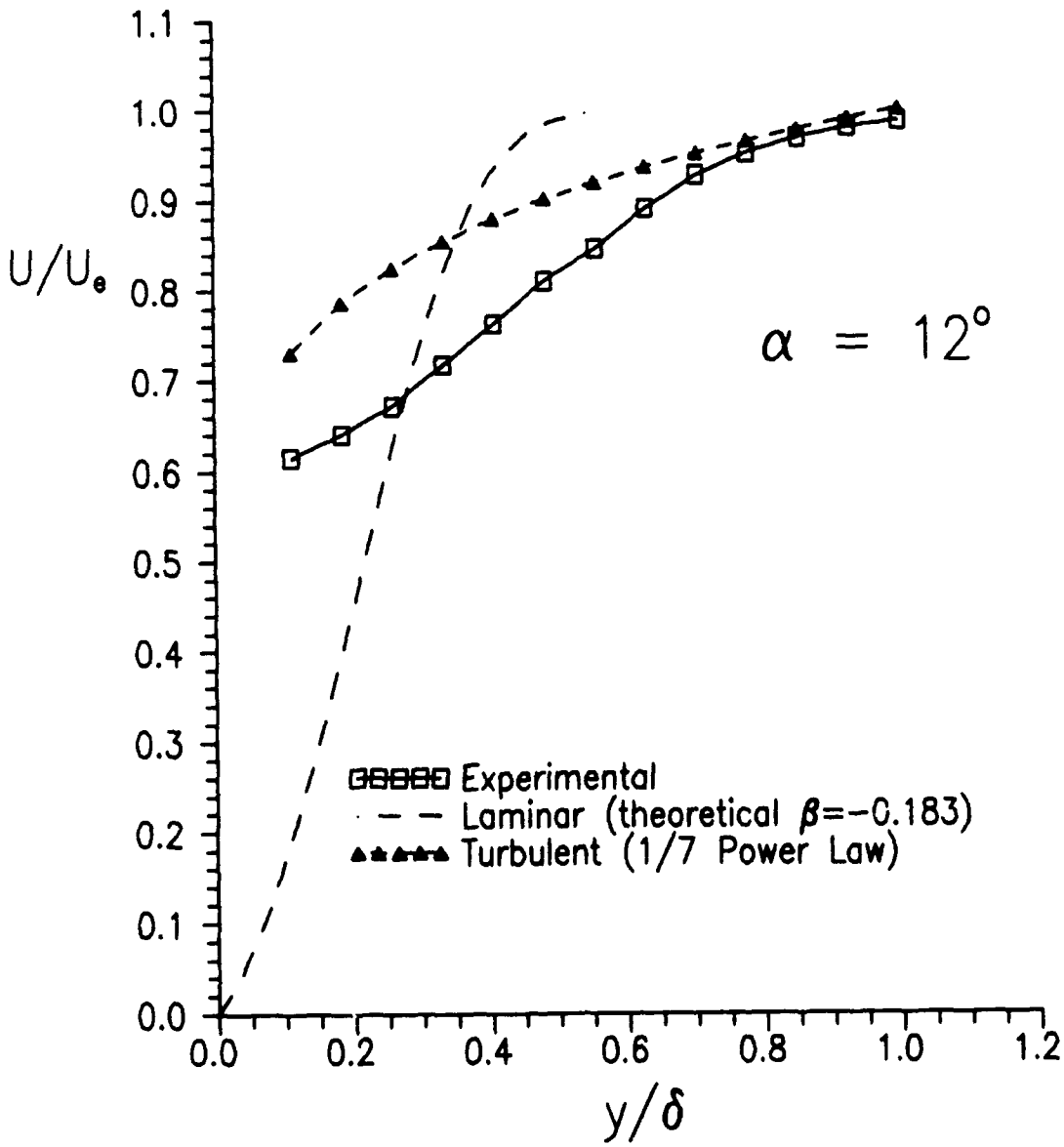

Fig. 40. Boundary Layer Profile (U_∞ = 80 ft/sec = 24.4 m/sec)

Appendix B: Experimental Data

TABLE III

Separation Locations - Cylinder

	U_∞ (ft/sec)	U_∞ (m/sec)	Re (x 10^4)	X_{sep} (in.)	Accuracy ± (in.)	ϕ_{sep} (deg)	h^+
	43.0	13.1	5.1	1.65	0.02	75.6	--
	49.4	15.1	5.9	1.84	0.02	84.3	--
	53.8	16.4	6.4	1.91	0.02	87.5	--
	58.3	17.8	6.9	1.96	0.02	89.8	--
No	62.0	18.9	7.2	1.97	0.02	90.3	--
Riblets	66.2	20.2	7.7	1.99	0.02	91.2	--
	69.1	21.1	8.0	2.00	0.02	91.7	--
	76.6	23.4	8.9	2.00	0.02	91.7	--
	84.0	25.6	9.7	2.00	0.02	91.7	--
	98.8	30.1	11.4	2.05	0.02	94.0	--
	110.3	33.6	12.7	2.05	0.02	94.0	--
	119.4	36.4	13.7	2.05	0.02	94.0	--
	42.5	12.9	5.1	1.70	0.05	77.9	10.9
	48.7	14.8	5.9	1.90	0.05	87.1	12.5
	53.5	16.3	6.4	1.95	0.02	89.4	13.9
	56.9	17.4	6.8	1.98	0.02	90.8	15.3
	61.2	18.7	7.3	2.00	0.02	91.7	16.7
	66.0	20.1	7.9	2.05	0.02	94.0	17.9
	67.8	20.7	8.2	2.06	0.02	94.4	18.6
	71.7	21.9	8.6	2.07	0.02	94.9	19.5
Riblets	75.0	22.9	9.0	2.09	0.02	95.8	20.2
	78.8	24.0	9.4	2.11	0.02	96.7	20.9
	81.2	24.8	9.6	2.11	0.02	96.7	21.5
	85.0	25.9	10.0	2.10	0.02	96.3	22.5
	89.9	27.4	10.6	2.10	0.02	96.3	23.7
	93.2	28.4	11.0	2.10	0.02	96.3	24.5
	98.0	29.9	11.6	2.10	0.02	96.3	25.8
	102.5	31.3	12.6	2.09	0.02	95.8	28.1
	107.9	32.9	13.2	2.07	0.02	94.9	29.3
	112.9	34.4	13.7	2.05	0.02	94.0	30.5
	119.8	36.5	14.5	2.05	0.02	94.0	32.2

TABLE IV

Pressure Distributions - Cylinder

	U_∞ (ft/sec)	44.4	48.2	--	57.0	59.3	63.2	--	71.6	--	--
	U_∞ (m/sec)	13.5	14.7	--	17.4	18.1	19.3	--	21.8	--	--
	Re (x 10^4)	5.4	5.8	--	6.9	7.1	7.5	--	8.5	--	--
No Riblets	ø (deg)				C_p						
	0	0.99	0.99	--	0.99	1.05	1.02	--	1.02	--	--
	30	0.38	0.35	--	0.35	0.48	0.46	--	0.47	--	--
	60	-1.18	-1.40	--	-1.40	-1.45	-1.41	--	-1.30	--	--
	90	-1.06	-1.46	--	-1.46	-1.44	-1.44	--	-1.37	--	--
	120	-1.06	-0.93	--	-0.93	-0.80	-0.82	--	-0.76	--	--
	150	-1.13	-0.90	--	-0.90	-0.83	-0.86	--	-0.79	--	--
	180	-0.94	-0.84	--	-0.84	-0.81	-0.82	--	-0.74	--	--
	U_∞ (ft/sec)	42.5	48.7	53.5	56.9	61.2	66.0	67.8	71.7	75.0	78.8
	U_∞ (m/sec)	12.9	14.8	16.3	17.4	18.7	20.1	20.7	21.9	22.9	24.0
	Re (x 10^4)	5.1	5.9	6.4	6.8	7.3	7.9	8.2	8.6	9.0	9.4
Riblets	ø (deg)				C_p						
	0	0.98	0.96	0.95	0.97	0.98	0.99	0.97	0.96	0.97	0.97
	30	0.31	0.33	0.31	0.30	0.34	0.34	0.31	0.33	0.33	0.35
	60	-1.11	-1.12	-1.19	-1.36	-1.44	-1.43	-1.41	-1.41	-1.37	-1.31
	90	-0.98	-0.96	-1.04	-1.23	-1.40	-1.35	-1.42	-1.37	-1.30	-1.28
	120	-1.06	-1.00	-0.98	-0.98	-0.91	-0.85	-0.85	-0.85	-0.82	-0.79
	150	-1.11	-1.04	-0.95	-0.97	-0.91	-0.84	-0.85	-0.85	-0.82	-0.79
	180	-1.00	-0.94	-0.91	-0.94	-0.88	-0.84	-0.85	-0.84	-0.82	-0.78

TABLE IV (Continued)

	U_∞ (ft/sec)	80.9	--	--	91.9	99.7	--	109.8	--	122.0	139.0
	U_∞ (m/sec)	24.7	--	--	28.0	30.4	--	33.5	--	37.2	42.4
	Re ($\times 10^4$)	9.6	--	--	10.9	11.7	--	12.9	--	14.3	16.2
No Riblets	ϕ (deg)				C_p						
	0	1.01	--	--	1.01	1.00	--	1.00	--	1.00	1.00
	30	0.45	--	--	0.44	0.43	--	0.43	--	0.42	0.43
	60	-1.29	--	--	-1.30	-1.31	--	-1.27	--	-1.25	-1.27
	90	-1.34	--	--	-1.31	-1.28	--	-1.27	--	-1.24	-1.23
	120	-0.74	--	--	-0.73	-0.73	--	-0.72	--	-0.71	-0.71
	150	-0.76	--	--	-0.74	-0.74	--	-0.74	--	-0.73	-0.73
	180	-0.73	--	--	-0.74	-0.74	--	-0.71	--	-0.70	-0.70
	U_∞ (ft/sec)	81.2	85.0	89.9	93.2	98.0	102.5	107.9	112.9	119.8	--
	U_∞ (m/sec)	24.8	25.9	27.4	28.4	29.9	31.3	32.9	34.4	36.5	--
	Re ($\times 10^4$)	9.6	10.0	10.6	11.0	11.6	12.6	13.2	13.7	14.5	--
Riblets	ϕ (deg)				C_p						
	0	0.98	0.97	0.96	0.99	0.97	0.99	0.99	0.98	0.99	--
	30	0.35	0.35	0.34	0.36	0.35	0.32	0.32	0.33	0.34	--
	60	-1.33	-1.34	-1.32	-1.31	-1.32	-1.33	-1.30	-1.30	-1.29	--
	90	-1.25	-1.22	-1.21	-1.19	-1.17	-1.02	-0.99	-0.99	-0.96	--
	120	-0.77	-0.78	-0.79	-0.78	-0.76	-0.77	-0.76	-0.77	-0.77	--
	150	-0.79	-0.79	-0.79	-0.78	-0.78	-0.78	-0.78	-0.77	-0.77	--
	180	-0.77	-0.76	-0.78	-0.78	-0.77	-0.77	-0.75	-0.75	-0.76	--

TABLE V

Separation Locations - Airfoil (α = 8 deg)

	U_∞ (ft/sec)	U_∞ (m/sec)	Re (x 10^4)	X_{sep} (in.)	Accuracy ± (in.)	$X_{sep/L}$	h^+
	41.8	12.7	5.1	1.55	0.02	0.60	--
	55.3	16.9	6.8	1.85	0.02	0.71	--
	72.1	22.0	8.8	2.00	0.02	0.77	--
No	80.4	24.5	9.8	2.05	0.02	0.79	--
Riblets	88.4	27.0	10.7	2.05	0.02	0.79	--
	96.1	29.3	11.5	1.95	0.02	0.75	--
	104.1	31.7	12.5	1.95	0.02	0.75	--
	110.7	33.8	13.2	1.95	0.02	0.75	--
	42.0	12.8	5.1	2.15	0.15	0.83	11.4
	55.5	16.9	6.6	2.15	0.05	0.83	14.5
	71.5	21.8	8.5	2.20	0.05	0.85	18.6
	80.9	24.7	9.5	2.15	0.05	0.83	20.7
Riblets	89.1	27.2	10.5	2.15	0.05	0.83	22.6
	97.7	29.8	11.4	2.15	0.05	0.83	24.6
	105.5	32.2	12.1	2.10	0.10	0.81	26.1
	112.5	34.3	12.8	2.05	0.10	0.79	27.6
	120.2	36.6	13.6	2.00	0.10	0.77	29.2

TABLE VI

Separation Locations - Airfoil (α = 12 deg)

	U_∞ (ft/sec)	U_∞ (m/sec)	Re (x 10^4)	X_{sep} (in.)	Accuracy ± (in.)	$X_{sep/L}$	h^+
	69.8	21.3	8.7	1.60	0.02	0.62	--
No	79.0	24.1	9.9	1.60	0.02	0.62	--
Riblets	87.9	26.8	10.8	1.60	0.02	0.62	--
	95.5	29.1	11.8	1.60	0.02	0.62	--
	105.6	32.2	12.1	1.60	0.02	0.62	--
	56.4	17.2	6.7	1.70	0.10	0.65	11.5
	72.0	21.9	8.5	1.65	0.05	0.64	14.0
	80.6	24.6	9.5	1.70	0.05	0.65	15.0
Riblets	90.1	27.5	10.5	1.75	0.10	0.67	16.1
	97.4	29.7	11.3	1.75	0.10	0.67	17.0
	107.9	32.0	12.2	1.70	0.10	0.65	18.3
	112.0	34.1	13.0	1.65	0.05	0.64	19.5
	118.7	36.2	13.7	1.60	0.05	0.62	20.6

TABLE VII

Pressure Distributions - Airfoil (α = 8 deg)

	U_∞ (ft/sec)	35.9	55.6	71.4	81.1	89.1	97.2	104.5	110.8	119.0	124.2
	Re (x 10^4)	4.4	6.8	8.6	9.8	10.7	11.6	12.4	13.0	13.9	14.4
	x/c					C_p					
	0.025	-1.84	-1.60	-1.61	-1.56	-1.58	-1.59	-1.57	-1.53	-1.52	-1.56
	0.080	-1.73	-1.79	-1.71	-1.72	-1.75	-1.72	-1.68	-1.62	-1.61	-1.63
No	0.160	-1.73	-1.33	-1.15	-1.09	-1.06	-1.05	-1.05	-1.04	-1.05	-1.06
Riblets	0.250	-1.27	-0.96	-0.98	-0.99	-0.99	-0.99	-0.97	-0.96	-0.95	-0.98
	0.400	-0.81	-0.80	-0.81	-0.80	-0.77	-0.76	-0.73	-0.73	-0.71	-0.75
	0.670	-0.32	-0.24	-0.24	-0.24	-0.23	-0.22	-0.22	-0.21	-0.20	-0.24
	0.770	-0.32	-0.16	-0.15	-0.11	-0.12	-0.14	-0.14	-0.14	-0.14	-0.07
	0.100	0.11	0.09	0.11	0.10	0.11	0.11	0.11	0.08	0.11	0.05
	0.250	-0.11	-0.16	-0.15	-0.17	-0.17	-0.17	-0.16	-0.18	-0.17	-0.22
	0.400	-0.32	-0.37	-0.34	-0.37	-0.37	-0.36	-0.36	-0.42	-0.37	-0.42
	0.600	-0.18	-0.24	-0.23	-0.27	-0.27	-0.26	-0.26	-0.26	-0.25	-0.31
	0.670	-0.18	-0.22	-0.17	-0.18	-0.18	-0.18	-0.18	-0.18	-0.17	-0.06

	U_∞ (ft/sec)	41.0	55.4	71.5	80.9	89.1	96.8	105.0	111.5	117.2	122.9
	Re (x 10^4)	4.8	6.6	8.5	9.6	10.5	11.6	12.5	13.2	13.8	14.7
	x/c					C_p					
	0.025	-1.85	-1.64	-1.51	-1.45	-1.40	-1.48	-1.47	-1.43	-1.42	-1.40
	0.080	-2.07	-1.90	-1.79	-1.73	-1.65	-1.58	-1.56	-1.51	-1.49	-1.45
	0.160	-1.96	-1.57	-1.24	-1.18	-1.16	-1.19	-1.18	-1.14	-1.13	-1.11
Riblets	0.250	-1.12	-1.10	-1.08	-1.06	-1.04	-1.05	-1.04	-1.01	-1.00	-0.97
	0.400	-1.09	-0.96	-0.84	-0.79	-0.73	-0.77	-0.77	-0.73	-0.72	-0.67
	0.670	-0.39	-0.33	-0.26	-0.25	-0.24	-0.29	-0.30	-0.29	-0.28	-0.26
	0.770	-0.25	--	--	--	--	-0.23	-0.25	-0.23	-0.24	-0.25
	0.100	0.34	0.26	0.24	0.22	0.21	0.19	0.17	0.19	0.18	0.17
	0.250	-0.20	-0.17	-0.19	-0.20	-0.21	-0.23	-0.24	-0.23	-0.23	-0.23
	0.400	-0.39	-0.39	-0.38	-0.41	-0.42	-0.42	-0.43	-0.42	-0.42	-0.42
	0.600	-0.20	-0.29	-0.29	-0.31	-0.32	-0.33	-0.34	-0.33	-0.34	-0.33
	0.670	-0.22	-0.24	-0.27	-0.26	-0.26	-0.26	-0.28	-0.26	-0.26	-0.26

TABLE VIII

Pressure Distributions - Airfoil (α = 12 deg)

	U_∞ (ft/sec)	37.2	56.2	71.6	81.2	89.0	97.0	103.8	109.7	118.5	123.6
	Re ($\times 10^4$)	4.6	6.8	8.6	9.8	10.7	11.5	12.3	12.9	13.8	14.3
	x/c					C_p					
	0.025	-1.48	-2.18	-2.07	-2.16	-2.16	-2.08	-2.00	-1.91	-1.84	-1.84
	0.080	-1.38	-2.13	-2.06	-2.09	-1.98	-1.87	-1.77	-1.69	-1.62	-1.63
No	0.160	-0.79	-1.57	-1.54	-1.27	-1.20	-1.15	-1.07	-1.06	-1.00	-1.01
Riblets	0.250	-0.69	-0.97	-0.96	-0.96	-0.94	-0.88	-0.82	-0.81	-0.75	-0.76
	0.400	-0.63	-0.71	-0.67	-0.62	-0.58	-0.51	-0.46	-0.49	-0.48	-0.50
	0.670	-0.63	-0.29	-0.30	-0.34	-0.34	-0.35	-0.39	-0.41	-0.43	-0.45
	0.770	-0.76	-0.29	-0.28	-0.30	-0.32	-0.33	-0.37	-0.39	-0.41	
	0.100	0.20	0.35	0.36	0.35	0.33	0.33	0.32	--	0.29	0.26
	0.250	-0.10	-0.01	-0.01	-0.04	-0.05	-0.04	-0.05	-0.06	-0.06	-0.11
	0.400	-0.33	-0.26	-0.26	-0.29	-0.29	-0.30	-0.29	-0.41	-0.32	-0.36
	0.600	-0.30	-0.23	-0.23	-0.26	-0.25	-0.26	-0.27	-0.28	-0.28	-0.33
	0.670	-0.33	-0.20	-0.17	-0.17	-0.19	-0.18	-0.21	-0.22	-0.21	-0.25

	U_∞ (ft/sec)	--	56.4	72.0	80.6	90.1	97.3	104.9	112.0	118.7	122.5
	Re ($\times 10^4$)	--	6.8	8.5	9.5	10.5	11.3	12.2	13.0	13.7	14.5
	x/c					C_p					
	0.025	--	-2.24	-2.05	-1.95	-1.83	-1.76	-1.67	-1.61	-1.54	-1.58
	0.080	--	-2.33	-2.17	-1.97	-1.56	-1.47	-1.38	-1.34	-1.31	-1.35
	0.160	--	-1.90	-1.32	-1.17	-1.00	-0.93	-0.89	-0.87	-0.85	-0.89
Riblets	0.250	--	-1.09	-0.93	-0.78	-0.65	-0.59	-0.60	-0.60	-0.60	-0.66
	0.400	--	-0.81	-0.58	-0.48	-0.45	-0.46	-0.46	-0.47	-0.49	-0.49
	0.670	--	-0.49	-0.43	-0.43	-0.47	-0.46	-0.47	-0.48	-0.50	-0.50
	0.770	--	-0.41	-0.38	-0.41	-0.44	-0.45	-0.46	-0.47	-0.49	-0.50
	0.100	--	0.38	0.42	0.41	0.38	0.37	0.37	0.36	0.35	0.35
	0.250	--	-0.13	-0.07	-0.09	-0.10	-0.11	-0.12	-0.13	-0.14	-0.13
	0.400	--	-0.38	-0.31	-0.33	-0.34	-0.36	-0.37	-0.38	-0.38	-0.38
	0.600	--	-0.34	-0.26	-0.30	-0.32	-0.33	-0.34	-0.36	-0.36	-0.36
	0.670	--	-0.27	-0.22	-0.26	-0.27	-0.27	-0.28	-0.30	-0.29	-0.29

Vita

Captain Timothy D. Wieck[redacted], [redacted] He graduated from Valley Lutheran High School in Saginaw, Michigan in 1980 and attended Embry-Riddle Aeronautical University, Daytona Beach, Florida on an AFROTC scholarship. He received a Bachelor of Science in Aeronautical Engineering in April 1984 and, as a Distinguished Graduate of AFROTC, received a commission in the USAF. Upon graduation, he was assigned to the Foreign Technology Division, Wright-Patterson AFB, as a Special Mission Aircraft Analyst until entering the School of Engineering, Air Force Institute of Technology, in June 1988.

[redacted]

UNCLASSIFIED
SECURITY CLASSIFICATION OF THIS PAGE

REPORT DOCUMENTATION PAGE

Form Approved
OMB No. 0704-0188

1a. REPORT SECURITY CLASSIFICATION UNCLASSIFIED	1b. RESTRICTIVE MARKINGS
2a. SECURITY CLASSIFICATION AUTHORITY	3. DISTRIBUTION/AVAILABILITY OF REPORT Approved for public release; distribution unlimited
2b. DECLASSIFICATION/DOWNGRADING SCHEDULE	
4. PERFORMING ORGANIZATION REPORT NUMBER(S) AFIT/GAE/ENY/89D-40	5. MONITORING ORGANIZATION REPORT NUMBER(S)
6a. NAME OF PERFORMING ORGANIZATION School of Engineering 6b. OFFICE SYMBOL (If applicable) AFIT/ENY	7a. NAME OF MONITORING ORGANIZATION
6c. ADDRESS (City, State, and ZIP Code) Air Force Institute of Technology (AU) Wright-Patterson AFB, OH 45433-6583	7b. ADDRESS (City, State, and ZIP Code)
8a. NAME OF FUNDING/SPONSORING ORGANIZATION 8b. OFFICE SYMBOL (If applicable)	9. PROCUREMENT INSTRUMENT IDENTIFICATION NUMBER
8c. ADDRESS (City, State, and ZIP Code)	10. SOURCE OF FUNDING NUMBERS PROGRAM ELEMENT NO. / PROJECT NO. / TASK NO / WORK UNIT ACCESSION NO.

11. TITLE (Include Security Classification)
EFFECT OF RIBLETS ON FLOW SEPARATION FROM A CYLINDER AND AN AIRFOIL IN SUBSONIC FLOW

12. PERSONAL AUTHOR(S)
Timothy D. Wieck, CPT, USAF

13a. TYPE OF REPORT	13b. TIME COVERED	14. DATE OF REPORT (Year, Month, Day)	15. PAGE COUNT
MS Thesis	FROM _____ TO _____	1989 December	83

16. SUPPLEMENTARY NOTATION

17. COSATI CODES			18. SUBJECT TERMS (Continue on reverse if necessary and identify by block number)
FIELD	GROUP	SUB-GROUP	Riblets, Airfoil, Flow separation, Cylinder
01	01		

19. ABSTRACT (Continue on reverse if necessary and identify by block number)

Thesis: LTC Paul I. King
Associate Professor
Department of Aeronautics and Astronautics

Abstract on back

20. DISTRIBUTION/AVAILABILITY OF ABSTRACT ☐ UNCLASSIFIED/UNLIMITED ☒ SAME AS RPT ☐ DTIC USERS	21. ABSTRACT SECURITY CLASSIFICATION UNCLASSIFIED
22a. NAME OF RESPONSIBLE INDIVIDUAL LTC Paul I. King, Assoc. Professor	22b. TELEPHONE (Include Area Code) (513) 255-3517 22c. OFFICE SYMBOL AFIT/ENY

DD Form 1473, JUN 86 — Previous editions are obsolete. — SECURITY CLASSIFICATION OF THIS PAGE

The purpose of this thesis was to investigate the effect of riblets on flow separation from a cylinder and an airfoil in subsonic flow. Riblets have been used successfully to reduce viscous drag on a flat plate and significantly delay flow separation in a two-dimensional, straight-walled, subsonic diffuser.

The investigation indicated that for a 2-D cylinder model, the separation point could be delayed as much as 5.5 percent by applying riblets to the model surface. Minor delays in separation were also achieved by applying riblets to a 2-D airfoil model at 8 and 12 deg angle of attack.

Applying riblets to the cylinder and airfoil models consistently altered the pressure distribution compared to the same models without riblets. In comparing the cylinder and airfoil results with those of the subsonic diffuser, it appears that riblets are most effective in delaying flow separation in relatively weak adverse pressure gradients.